Progress in Oceanography 213 (2023) 102996

Contents lists available at ScienceDirect

Progress in Oceanography

journal homepage: www.elsevier.com/locate/pocean

Seasonal plankton dynamics in Kongsfjorden during two years of contrasting environmental conditions

Philipp Assmy [a,*], Ane Cecilie Kvernvik [a], Haakon Hop [a], Clara J.M. Hoppe [b], Melissa Chierici [c,d], Divya David T. [e], Pedro Duarte [a], Agneta Fransson [a,d], Laura M. García [a,f], Weronika Patuła [g], Sławomir Kwaśniewski [g], Marion Maturilli [h], Olga Pavlova [a], Agnieszka Tatarek [g], Jozef M. Wiktor [g], Anette Wold [a], Klara K.E. Wolf [b,i], Allison Bailey [a]

[a] Norwegian Polar Institute, Fram Centre, 9296 Tromsø, Norway
[b] Alfred Wegener Institute, Helmholtz Centre for Polar and Marine Research, 27570 Bremerhaven, Germany
[c] Institute of Marine Research, Fram Centre, 9296 Tromsø, Norway
[d] University Centre in Svalbard, 9171 Longyearbyen, Norway
[e] National Center for Polar and Ocean Research, Ministry of Earth Sciences, Vasco da Gama, 403804 Goa, India
[f] UiT - The Arctic University of Norway, Department of Arctic and Marine Biology, Tromsø, Norway
[g] Institute of Oceanology, Polish Academy of Sciences, 81-712 Sopot, Poland
[h] Alfred Wegener Institute, Helmholtz Centre for Polar and Marine Research, 14773 Potsdam, Germany
[i] University of Hamburg, Institute of Marine Ecosystem and Fishery Science, 22767 Hamburg, Germany

ARTICLE INFO

Keywords:
Arctic Ocean
Kongsfjorden
Seasonality
Protist plankton
Zooplankton
Phaeocystis
Diatoms

ABSTRACT

Seasonal plankton time-series data are presented from Kongsfjorden from two years with contrasting environmental conditions. Kongsfjorden (west coast of Spitsbergen – 79°N) integrates inputs from Atlantic and Arctic waters, and glacier run-off, and is thus a prime location to study impacts on ecosystem dynamics of key environmental drivers that are relevant across the Arctic. Despite extensive research in Kongsfjorden, seasonally-resolved data are scarce. From late April/early May to early September 2019 and 2020, we conducted pelagic sampling at a mid-fjord station at mostly weekly to bi-weekly resolution investigating the environmental drivers of phyto- and zooplankton community composition and phenology. During spring 2019, Atlantic water masses with temperatures > 1 °C were found throughout the upper 250 m of the water column, and little sea ice occurred in the fjord. Spring 2020, in turn, was characterized by the presence of local water masses with sub-zero temperatures and relatively extensive sea-ice cover. The most striking contrast between the two years was the difference in phytoplankton spring bloom composition. In 2019, the spring bloom was dominated by the colonial stage of the haptophyte *Phaeocystis pouchetii* and diatoms played a minor role, while the spring bloom in 2020 was dominated by diatoms of the genus *Thalassiosira* succeeded by *P. pouchetii*. Selective grazing by large copepods and water mass structure seem to have been the decisive factors explaining the marked difference in diatom spring bloom biomass between the years while similar spring abundances of *P. pouchetii* in both years indicated that this species was less impacted by those factors. Our data suggest that differences in spring bloom composition impacted trophic transfer and carbon export. Recruitment of the dominant copepods *Calanus finmarchicus* and *C. glacialis*, Cirripedia and euphausiid larvae as well as the export of carbon to the seabed was more efficient during the diatom-dominated compared to the *P. pouchetii*–dominated spring bloom. In summer, the plankton composition shifted towards a flagellate-dominated community characterized by mixo- and heterotrophic taxa adapted to a lower nutrient regime and strong top-down control by copepod grazers. However, residual silicic acid after the *P. pouchetii*–dominated spring bloom fueled a late summer diatom bloom in 2019.

Our data provide a first glimpse into the environmental drivers of plankton phenology and underline that high-resolution monitoring over many annual cycles is required to resolve the ephemeral variations of plankton populations against the backdrop of climate change.

* Corresponding author.
E-mail address: Philipp.Assmy@npolar.no (P. Assmy).

https://doi.org/10.1016/j.pocean.2023.102996
Received 14 July 2022; Received in revised form 19 December 2022; Accepted 20 February 2023
Available online 24 February 2023
0079-6611/© 2023 The Author(s). Published by Elsevier Ltd. This is an open access article under the CC BY license (http://creativecommons.org/licenses/by/4.0/).

1. Introduction

Climate change is expected to have diverse impacts on the Arctic marine ecosystem. These include an increase in pelagic net primary production and earlier timing of the phytoplankton spring bloom in Arctic waters as a result of a longer open-water season (Arrigo and van Dijken, 2015; Ardyna and Arrigo, 2020; Dalpadado et al., 2020; Ingvaldsen et al., 2021) which can result in mismatches in the timing of primary production and the reproductive cycle of key Arctic zooplankton grazers (Søreide et al., 2010). In addition, increased meltwater-induced stratification in summer is projected to lead to a dominance of smaller phytoplankton species (Li et al., 2009). These small-sized phytoplankton (<3–20 μm) are considered a less nutritive and accessible food source for the large, lipid-rich Arctic zooplankton grazers (Piwosz et al., 2015) and contribute less to carbon export to the seafloor than the larger diatoms (Wiedmann et al., 2020). The northward range expansion of boreal species, ranging from cyanobacteria (Paulsen et al., 2016), to coccolithophores (Oziel et al., 2020), fish (Berge et al., 2015, Fossheim et al., 2015), seabirds (Descamps and Strøm 2021) and mammals (Lefort et al., 2020) could also potentially have negative consequences for local Arctic flora and fauna.

Fjords and coastal waters are among the most productive in the Arctic (Piwosz et al., 2009; Hodal et al., 2012; Duarte et al., 2019), provide valuable ecosystem services based on food webs supporting top trophic levels (e.g. marine mammals and seabirds) with associated tourism industry (Hovelsrud et al., 2021) and play an important role for biogeochemical cycles (Lalande et al., 2016). The archipelago of Svalbard in the European Arctic is one of the fastest changing regions in the Arctic (Hanssen-Bauer et al., 2019) with increasing air and water temperatures (Hop et al., 2019a; Maturilli et al., 2019; Isaksen et al., 2022), increasing precipitation, including rain events in winter (Hanssen-Bauer et al., 2019), Atlantification and increased water column stratification (Prominska et al., 2017; Tverberg et al., 2019), coastal water darkening (Konik et al., 2021), as well as decreasing landfast sea ice (Pavlova et al., 2019; Søreide et al., 2020) and retreating glaciers (Østby et al., 2017). Svalbard fjords host diverse marine ecosystems (Duarte et al., 2019; Søreide et al., 2020) and are important foraging and breeding areas for invertebrates, fish, seabirds and marine mammals (Lydersen et al., 2014; Descamps et al., 2017). The ecosystem functioning and services are ultimately dependent on the energy provision at the base of the marine food web provided by primary (phytoplankton) and secondary (zooplankton) producers (Hegseth et al., 2019; Hop et al., 2019b). Thus, it is important to improve our understanding of the ecosystem drivers of phyto- and zooplankton composition and development in a rapidly changing environment.

Kongsfjorden is an established research site on the west coast of Spitsbergen and one of the best studied marine systems in the Arctic (Hop and Wiencke, 2019) that integrates inputs from Atlantic and Arctic water masses (Tverberg et al., 2019), and glacier run-off (Fransson et al., 2016; Halbach et al., 2019). It is therefore a suitable area to study climate change impacts on marine ecosystem dynamics, including the timing, magnitude and species composition of protist and zooplankton communities, which apply to a wider region of the Atlantic–influenced Arctic (Bischof et al., 2019). Long-term observations of pelagic ecosystems in Svalbard waters have revealed seasonal and interannual patterns in phytoplankton bloom composition and timing or zooplankton phenology (Seuthe et al., 2011; Gluchowska et al., 2016; Ormanczyk et al., 2017; Kubiszyn et al., 2017; Hegseth et al., 2019; Hop et al., 2019a; Dabrowska et al., 2021). However, despite the extensive marine research in Kongsfjorden over the last decades, seasonally-resolved data on marine ecosystem dynamics are sparse (but see Walkusz et al., 2009; Rokkan Iversen and Seuthe, 2011; van de Poll et al., 2020, 2021; Dabrowska et al., 2021). Indeed, a lack of seasonally-resolved sampling and long-term datasets were identified as key limitations for implementing plankton indicators of Good Environmental Status for Arctic pelagic habitats compliant with the EU Marine Strategy Framework Directive OSPAR as developed for the Northeast Atlantic (Siddons et al., 2018). Overcoming these knowledge gaps is a prerequisite to advance our understanding of coastal Arctic ecosystems and how changes at the base of the marine food web translate into trophic transfer and the strength of the biological carbon pump.

In 2019, the Norwegian Polar Institute established the Kongsfjorden long-term seasonal pelagic monitoring program based at the Ny-Ålesund Research Station. It aims to observe timing, duration, magnitude and composition of the phytoplankton spring bloom, the match or mismatch with zooplankton grazers, and impacts of environmental factors, including meltwater run-off during summer, on the plankton community. Here we present seasonal data on hydrography, seawater chemistry, protists, and zooplankton from spring to early autumn in Kongsfjorden from the first two years of the long-term seasonal pelagic monitoring program. The aim of this study is to evaluate year to year changes in abiotic conditions in relation to planktonic community composition and timing to improve our understanding of pelagic ecosystem functioning under contrasting environmental conditions that could be representative of the climatic changes observed in the Arctic.

2. Materials and methods

2.1. Study area

This study was conducted in Kongsfjorden, an approximately 4 – 10 km wide and 20 km long fjord located on the west coast of Spitsbergen, Norway (78°58′N, 11°51′E; Fig. 1). Kongsfjorden lacks a sill at its mouth and is thus open for advection of water masses from the adjacent shelf area. Water masses on the West Spitsbergen shelf are a mixture of warm and saline Atlantic water (AW, >3°C, >34.65), colder and fresher Arctic water (ArW, −1.5–1.0 °C, 34.30–34.80) and freshwater from glacier melt and terrestrial runoff. The AW mixes with ArW on the shelf, and is advected into Kongsfjorden as Transformed Atlantic Water (TAW, 1.0–3.0 °C, >34.65) (Svendsen et al., 2002; Cottier et al., 2005). During autumn and winter, Local Water (LW) and Winter Cooled Water (WCW) are formed in the fjord through surface cooling and convection. Local Water is characterized by a temperature range of −0.5–1.0 °C and a salinity range of 34.30–34.85 dependent on the water present in the fjord at the end of the summer. The very cold (<-0.5 °C) and dense WCW results from sea-ice formation and associated convection during intense cooling (Cottier et al., 2005). A 20 m deep sill (around the Lovénøyane islands) separates the shallow inner part of the fjord (<100 m) from the deeper outer part (>300 m). The inner fjord is lined by tidewater glaciers (Kongsvegen, Kronebreen, Kongsbreen and Conwaybreen) and is heavily impacted by glacier run-off during the melt season. The water masses in Kongsfjorden often change seasonally between a state of Atlantic dominance (warm and saline) and Arctic dominance (colder and fresher).

2.2. Field sampling

From late April/early May to early September 2019 and 2020, respectively, we took CTD measurements and collected samples for seawater chemistry, as well as protist plankton and zooplankton taxonomy and abundance at a mid-fjord station (Kb3; 78°57.228′N, 11°57.192′E; ~ 340 m deep). Plankton and hydrography have been monitored at Kb3 annually in summer since 1996, and the station is representative of the deep outer fjord basin while also being close to the research settlement Ny-Ålesund (Hop et al., 2002; Hop and Wiencke, 2019). Pelagic sampling at station Kb3 was conducted at weekly intervals in 2019 (19 sampling events) and less frequently in 2020 (12 events) from a small vessel, MS *Teisten* (Kings Bay AS, Ny-Ålesund). Sampling was done from larger vessels on 9 August 2019 (RV *Lance*) and on 28 July 2020 (RV *Kronprins Haakon*). Detailed information on sampling dates, bloom stage (defined in the protist taxonomy section), mixed layer and euphotic zone depth is shown in Table 1. On each

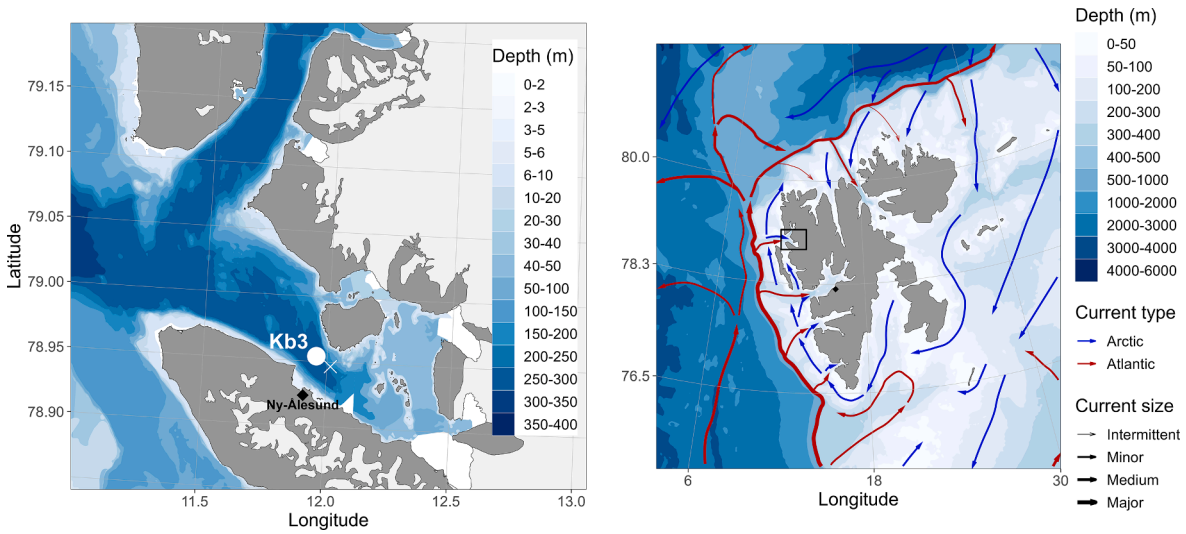

Fig. 1. The Svalbard archipelago with Atlantic water currents in red and Arctic water currents in blue (right panel) and close-up of Kongsfjorden on the west coast of Spitsbergen (left panel). Sampling was conducted at a mid-fjord station (Kb3) from late April/early May to early September in 2019 and 2020. The position of the Ny-Ålesund Research Station and the IndARC mooring are marked with a black diamond and white X on the Kongsfjorden map. Longyearbyen is marked with a black diamond on the Svalbard map. The map uses bathymetry from the Norwegian Mapping Authority and Jakobsson et al. (2012) and land shapefiles from the Norwegian Polar Institute © as described in Vihtakari (2020). (For interpretation of the references to color in this figure legend, the reader is referred to the web version of this article.)

Table 1
Sampling dates, bloom stage/season, euphotic zone depth (Z; defined as the 1% light depth relative to incoming irradiance, in meters), mixed layer depth (MLD, in meters), and sampled parameters (CTD = CTD profile, NUT = nutrients, DIC = dissolved inorganic carbon, POC/N = particulate organic carbon and nitrogen, CHL = chlorophyll *a*, PHT = phytoplankton, ZOT = zooplankton).

Date	Bloom stage/season	Z(1%)	MLD	Sampled parameters
2019				
26 April	Early bloom	NA	150	CTD, NUT, DIC, POC/N, CHL, PHT, ZOT
29 April	Early bloom	23.5	150	CTD, NUT, DIC, POC/N, CHL, PHT, ZOT
7 May	Early bloom	23.5	150	CTD, NUT, DIC, POC/N, CHL, PHT, ZOT
13 May	Early bloom	23.5	150	CTD, NUT, DIC, POC/N, CHL, PHT, ZOT
20 May	Peak Bloom	17.6	150	CTD, NUT, DIC, POC/N, CHL, PHT, ZOT
27 May	Peak Bloom	NA	135	CTD, NUT, DIC, POC/N, CHL, PHT, ZOT
3 June	Peak Bloom	NA	14	CTD, NUT, DIC, POC/N, CHL, PHT, ZOT
10 June	Post-bloom	NA	22	CTD, NUT, DIC, POC/N, CHL, PHT, ZOT
20 June	Post-bloom	13.2	21	CTD, NUT, DIC, POC/N, CHL, PHT, ZOT
24 June	Post-bloom	11.2	15	CTD, NUT, DIC, POC/N, CHL, PHT, ZOT
3 July	Post-bloom	4.2	22	CTD, NUT, DIC, POC/N, CHL, PHT, ZOT
9 July	Summer	6.9	16	CTD, NUT, DIC, POC/N, CHL, PHT, ZOT
15 July	Summer	6.1	37	CTD, NUT, DIC, POC/N, CHL, PHT, ZOT
22 July	Summer	8.9	5	CTD, NUT, DIC, POC/N, CHL, PHT, ZOT
29 July	Summer	6.1	17	CTD, NUT, DIC, POC/N, CHL, PHT, ZOT
6 August	Summer	9.1	20	CTD, NUT, DIC, POC/N, CHL, PHT, ZOT
26 August	Autumn	11.5	15	CTD, NUT, DIC, POC/N, CHL, PHT, ZOT
2 September	Autumn	13.6	20	CTD, NUT, DIC, POC/N, CHL, PHT, ZOT
2020				
1 May	Early bloom	NA	NA	CTD, CHL, PHT
6 May	Early bloom	NA	NA	CTD, CHL, PHT
8 May	Early bloom	NA	7	CTD, NUT, DIC, POC/N, CHL, PHT, ZOT
12 May	Peak Bloom	24.2	7	CTD, NUT, DIC, POC/N, CHL, PHT, ZOT
14 May	Peak Bloom	NA	NA	CTD
19 May	Peak Bloom	26.3	26	CTD, NUT, DIC, POC/N, CHL, PHT, ZOT
22 May	Peak Bloom	NA	NA	CTD, NUT, CHL, PHT
25 May	Peak Bloom	18.5	22	CTD, NUT, DIC, POC/N, CHL, PHT, ZOT
28 May	Post-bloom	NA	102	CTD, NUT
4 June	Post-bloom	19.7	97	CTD, NUT, DIC, POC/N, CHL, PHT, ZOT
9 June	Post-bloom	NA	21	CTD, NUT, DIC, POC/N, CHL, PHT, ZOT
17 June	Post-bloom	30.2	19	CTD, NUT, DIC, POC/N, CHL, PHT, ZOT
16 July	Summer	NA	3	CTD
28 July	Summer	NA	7	CTD, NUT, DIC, POC/N, CHL, PHT, ZOT
12 August	Summer	NA	26	CTD
2 September	Autumn	18.5	12	CTD, NUT, DIC, POC/N, CHL, PHT, ZOT
8 September	Autumn	NA	10	CTD, NUT, DIC, POC/N, CHL, PHT, ZOT

sampling event, vertical profiles of salinity, temperature, chlorophyll *a* (Chl *a*) fluorescence and turbidity were obtained using a STD profiler (MiniSTD model SD-204, SAIV A/S, Bergen, Norway). Turbidity is given as a relative measure in Formazin Turbidity Units (FTU) based on the measurement of incident light scattered at right angles from the sample by a photodiode which produces an electronic signal that is converted to turbidity. *In situ* Chl *a* fluorescence was calibrated with Chl *a* data obtained from discrete samples (see below).

Water samples for Chl *a*, particulate organic carbon (POC) and nitrogen (PON), dissolved inorganic carbon (DIC), nutrients, and protist taxonomy and abundance were collected with 10 L Niskin bottles (Ocean Test Equipment Inc., Fort Lauderdale, FL., USA). Nutrient and DIC samples were collected at 5, 15, 25, 50, 150, and 300 m while Chl *a*, POC, PON and phytoplankton samples were taken at 5, 15, 25, and 50 m. DIC samples were transferred directly from the Niskin bottles into 250 mL clean borosilicate bottles using silicon tubing, after overflowing with two bottle volumes. Samples were preserved with saturated mercuric chloride (60 µl $HgCl_2$) within 4 h of sampling and stored dark at 4 °C until post-cruise analysis. Nutrient samples were filtered using 0.2 µm syringe-filters (Whatman SFCA, UK) that were pre-rinsed with the sample, and stored in 15 mL sample-rinsed Falcon tubes at −20 °C until analysis. For Chl *a* and POC and PON analyses, water from each depth was transferred directly into 1 L brown plastic bottles and kept cool while brought to the Marine lab in Ny-Ålesund for filtering within several hours of collection, or filtered immediately on board RV *Lance* and RV *Kronprins Haakon*. Samples for protist community composition were collected in 200 mL amber glass bottles, preserved with 25% glutaraldehyde and 20% hexamethylenetetramine-buffered formalin solution at final concentrations of 0.1 and 1%, respectively and kept cold (4 °C) until analysis. Most of the samples for meso- and macrozooplankton community composition (hereinafter referred to as "zooplankton") were collected from MS *Teisten* using vertical hauls with the WP-2 net (Hydro-Bios, Kiel, Germany) with 200 µm gauze in discrete layers from different depth strata (2019: 0 – 50 m, 0 – 100 m, and 0 – 300 m; 2020: 0 – 50 m, 50 – 100 m, and 100 – 300 m) at hauling speed of 0.5 m s^{-1}. In 2020 a mechanical device was used for net closing. The volume sampled with the WP-2 net is calculated based on the net's opening (0.2550 m^2) multiplied by the depth layer sampled. The zooplankton samples from RV *Lance* and RV *Kronprins Haakon* were collected using a MultiNet Midi (Hydro-Bios, Kiel, Germany) consisting of five nets with 0.25 m^2 opening and 200 µm gauze hauled vertically at a speed of 0.5 m s^{-1}. The depth strata sampled with the MultiNet were: 0–20 m, 20–50 m, 50–100 m, 100–200 m, and 200 m–bottom. The volume sampled was calculated based on regression using data from previous studies (sample volume = -1.2681 + 0.3298 * (maximum depth - minimum depth)). The WP-2 net and MultiNet are suited to catch the meso-zooplankton fraction, but larger macrozooplankton might escape the net and are likely underrepresented (Skjoldal et al., 2013; Ormanczyk et al., 2017). The content of the cod-end was collected on a sieve (200 µm) and gently flushed with filtered seawater before transfer into 125 mL plastic bottles and fixed with 37% hexamethylenetetramine-buffered formalin solution (4% final concentration).

Temperature and salinity data from a hydrographic mooring in vicinity of Kb3 (subsurface mooring 'IndARC' deployed by the National Centre for Polar and Ocean Research, India: 78°56.789′N, 12°00.889′E; ~ 198 m deep, Fig. 1) from January to September in 2019 and 2020 were used to investigate the water-mass conditions imprinting on the plankton community.

2.3. Environmental properties

2.3.1. Meteorological data

Average wind speed and direction as well as incoming incident photosynthetically active radiation (PAR) were measured close to the AWIPEV Atmospheric Observatory in Ny-Ålesund (Maturilli et al., 2019). A ThiesClima combined classic wind sensor was used to derive hourly-averaged wind speed (m s^{-1}) and direction (°) at 10 m above ground. Hourly-averaged incoming PAR (370 – 695 nm) was calculated by subtracting UV and IR spectrum from the global incoming radiation, measured using pyranometers with different shading domes (Maturilli et al., 2019). Data were converted from (W m^{-2}) to (µmol photons m^{-2} s^{-1}).

2.3.2. Mooring data

The CTD sensor (SBE 37-IMP MicroCAT; Seabird Scientific) attached to the mooring measured water temperature (°C) and salinity at discrete depths at hourly intervals. The accuracy of the temperature sensor was 0.002 °C for a range of −5 to 35 °C, and that of conductivity, from which the salinity is derived, is 0.0003 S m^{-1}. The deployments and retrievals of the mooring were done during mid-July each year. We used the temperature and salinity data from the mooring collected from January to 13 July in 2019 at 58, 87, 109, 150, and 168 m nominal depths. The mooring was recovered on 14 July 2019 and re-deployed on 17 July 2019 for the rest of the period to September 2020 in which the temperature and salinity data were recorded at 17, 50, 100, 150, and 180 m nominal depths. The gap of three days between the recovery and re-deployment was linearly interpolated. The data at 17 m were collected by a standard RBR Concerto CTD of the same accuracy as the SBE 37-IMP MicroCAT.

2.3.3. Sea-ice observations

Sea-ice cover in Kongsfjorden was registered by video recordings from the mountain Zeppelinfjellet (474 m a.s.L., south of Ny-Ålesund) or by direct observations during ice surveys (Gerland and Renner, 2007; Pavlova et al., 2019). Sea-ice extent monitoring in Kongsfjorden is a part of the Norwegian Polar Institute's long-term monitoring of Svalbard sea ice and the data are openly available (Gerland et al., 2022). The observations by video camera are weather and visibility permitting, and typically conducted several times a week from the onset of daylight sufficient for visual observations (February) and lasting until the end of the ice season in the fjord (June). Sea-ice extent data are derived mainly from hand-drawn ice maps and photography in selected observation areas. The ice is classified as landfast ice and 'other ice', which is usually either pack ice broken off the fast ice, or sea ice advected from other areas (Krossfjorden and areas outside Krossfjorden/Kongsfjorden).

2.3.4. Mixed layer depth

Mixed layer depth was approximated using temperature and salinity data obtained with the ship-based CTD profiles, which were used to calculate Brunt–Väisälä Frequency profiles:

$$N = \sqrt{(-g|\rho)*(-\Delta\rho|\Delta z)} \quad (1)$$

where g is the local acceleration of gravity (9.83 m s^{-1} for Ny-Ålesund), ρ the potential density (kg m^{-3}) and z the measurement depth (m). As higher values in N are indicative of higher water column stratification (Carvalho et al., 2017), the depth of subsurface maxima in N were defined as the mixed layer depth (MLD). In cases where several peaks were visible in the N profile, the peak most closely aligned with the Chl *a* maximum was used.

2.3.5. Euphotic zone depth

In 2019, vertical distribution of PAR was measured with an upward facing spherical quantum sensor (LI-COR LI-193, logger LI-1500) down to a depth of flux < 2 µmol photons m^{-2} s^{-1}. The euphotic zone depth was calculated as the depth of 1% of incident PAR measured with the surface reference sensor. Due to the lack of a PAR sensor in 2020, the euphotic zone depth was estimated with a Secchi disk according to Luhtala and Tolvanen (2013).

2.4. Biogeochemical properties

Nutrient samples were thawed for 24 h and analyzed

colourimetrically for nitrate (NO_3), nitrite (NO_2), silicic acid ($Si(OH)_4$), and phosphate (PO_4) on a QuaAAtro autoanalyzer (Seal Analytical, Mequon, USA) using internal calibrations and Certified Reference Materials (KANSO, Osaka, Japan) for quality control. Detection limits were 0.2 μmol L^{-1} for NO_3, 0.01 μmol L^{-1} for NO_2, 0.02 μmol L^{-1} for $Si(OH)_4$, and 0.02 μmol L^{-1} for PO_4.

Seawater samples for DIC were analyzed after the cruise at the Institute of Marine Research, Tromsø. Following methods outlined in Dickson et al. (2007), determination of DIC was carried out by gas extraction of acidified samples followed by coulometric titration and photometric detection (Johnson et al., 1987) using a Versatile Instrument for the Determination of Titration carbonate (VINDTA 3D, Marianda, Germany). Measurements were calibrated against Certified Reference Materials (CRM, provided by A. G. Dickson, Scripps Institution of Oceanography, USA). The DIC uncertainty was estimated to < 3 μmol kg^{-1} based on replicate analyses of CRMs.

Seawater samples for Chl *a* determination were filtered onto GF/F filters (Whatman, Maidstone, UK) using a gentle vacuum. Filters were extracted directly in 5 mL methanol (>99.9%) for 12 h at 4 °C in the dark (Holm-Hansen and Riemann, 1978). Chlorophyll *a* concentrations in extracts were measured on a Trilogy Laboratory fluorometer (Turner Designs, CA, USA) before, and after acidification with two drops of 5% HCl (Holm-Hansen and Riemann 1978). The measured concentrations of Chl *a* for 5, 15, 25, and 50 m depths were subsequently used to calibrate fluorescence-derived Chl *a* from vertical CTD profiles ($n = 68$; $r^2 = 0.92$). Maximum Chl *a* concentrations measured between 0 and 5 m were projected to the surface, to correct for fluorescence quenching by high actinic irradiances down to 5 m depth (Xing et al. 2012).

For POC/N analysis, seawater was filtered onto pre-combusted (12 h, 450 °C) GF/F filters, placed into Pall filter slides and dried at 60 °C for ~ 12 h in a drying oven. Filters were then acidic-fumed with HCl to remove carbonates and dried for at least 12 h at 60 °C. Samples collected in 2019 were analyzed at the Finnish Environment Institute with continuous-flow mass spectrometry (CF-IMRS) carried out with a roboprep/tracermass mass spectrometer (Europa Scientific, UK). All values have been corrected for instrument drift and glycine has been used as a reference standard. Samples collected in 2020 were analyzed at the Alfred Wegener Institute. Analysis was performed using a CHNS-O elemental analyser (Euro EA 3000, HEKAtech) using different amounts of acetanilide as a calibration standard. Concentrations of POC and PON were corrected for blank measurements and normalized to filtered volume.

Depth-integrated standing stocks of Chl *a*, POC/N, protist carbon (PC), DIC and nutrient inventories (mg m^{-2}, g m^{-2} or mmol m^{-2}) were calculated via numerical integration over 0–50 m using the trapezoidal rule.

2.5. Protist taxonomy

Protists were identified and counted, according to the Utermöhl method (Utermöhl, 1958; modified by Edler and Elbrächter, 2010), at 100x and 600x magnification on an inverted light microscope (Nikon Ti-S) equipped with differential interference contrast. At least 50 cells of the dominant species were counted (error of ± 28% according to Edler and Elbrächter, 2010) in each Utermöhl chamber. Organisms were identified to the lowest possible taxonomic level (Bérard-Therriault et al., 1999; Hasle and Heimdal, 1998; Okolodkov, 1993; Tomas, 1997; Throndsen et al. 2007; Wiktor et al., 1995).

Abundances were converted to carbon biomass based on published geometric relationships for biovolume conversion (Hillebrand et al., 1999) and biovolume to carbon conversion factors (Menden-Deuer and Lessard, 2000). Protist community compositions are reported as depth-specific abundances [cells L^{-1}] and biomass [μg C L^{-1}], as well as integrated over the upper 50 m of the water column (standing stocks as g C m^{-2}). In this study the bloom period was defined from standing stocks of protist biomass and was divided in three phases: Early bloom (before peak bloom; biomass < 4 g C m^{-2}), peak bloom (biomass > 4 g C m^{-2}) and post bloom (after peak bloom; biomass < 4 g C m^{-2}).

2.6. Zooplankton taxonomy

Zooplankton were identified and counted under a stereomicroscope equipped with an ocular micrometer, according to standard procedures (Postel et al., 2000; Kwasniewski et al., 2003). In the laboratory, each zooplankton sample was first screened for macrozooplankton (organisms > 5 mm overall length) all of which were selected, identified and counted. The remaining mesozooplankton size fraction was examined for taxonomic composition and abundance by a subsampling method (Postel et al., 2000). Subsamples of 2 mL volume were taken using a macropipette whose tapered tip was cut off, which ensured free suction of organisms up to 5 mm in length (an equivalent of the Stempel pipette) and all organisms in each subsample were identified and counted. Subsampling was continued until at least 500 individuals per sample were identified (Postel et al., 2000). *Calanus* spp. were identified to species level for each developmental stage based on prosome length (Kwasniewski et al., 2003). Other zooplankters were identified to the lowest possible taxonomic level based on available literature (see Table S1).

Zooplankton data is presented as abundance (ind. m^{-3}) in the different depth strata (2019: 0 – 50 m, 0 – 100 m, and 0 – 300 m; 2020: 0 – 50 m, 50 – 100 m, and 100 – 300 m) as well as dry mass (DM) via numerical integration over 0–300 m using the trapezoidal rule. The dry mass conversion factors were taken from Hop et al. (2019a) with subsequent updates (Table S1).

2.7. Spearman rank correlation analysis

In order to elucidate trophic relationships within the plankton community during the bloom period we performed a Spearman rank correlation analysis between depth-integrated abundances of the major protist and zooplankton groups during the early, peak and post bloom phases. The Spearman rank correlation measures the non-linear strength of association between two ranked variables, where a negative correlation is indicative of top-down control, while a positive correlation is indicative of bottom-up control. Correlations were deemed significant if they had a p-value < 0.05.

3. Results

3.1. Atmospheric forcing

Hourly-averaged incident PAR reached peak values of > 1200 μmol photons m^{-2} s^{-1} in late June and declined to < 200 μmol photons m^{-2} s^{-1} by the end of September (Fig. 2a, b). A similar range in PAR values was observed on a diurnal basis during the midnight sun period from mid-April until the end of August. In April, incoming PAR was higher in 2020 than in 2019, while the opposite was true for late May. The observed differences were the result of variable cloud cover. The remainder of the summer and early autumn values of incoming PAR were quite similar except for the second half of July 2019 when values were low.

Air temperatures stayed largely below 0 °C from January until mid-April in both years, with more and longer temperature excursions close to 0 °C in 2019 than in 2020, and above 0 °C from early May until the end of September, with peak temperatures of > 10 °C in July (Fig. 2c, d). The winter and spring were generally colder in 2020 than 2019, particularly the period from mid-March to mid-April 2020.

In terms of wind speed, July and August were the calmest periods in 2019 and 2020, respectively (Fig. 2e, f). As wind speed is related to passing cyclones, peak wind speeds > 10 m s^{-1} are less likely to occur during summer when cyclonic activity is lower. Strong northwesterly winds were prevalent from April to June 2019 and from February to

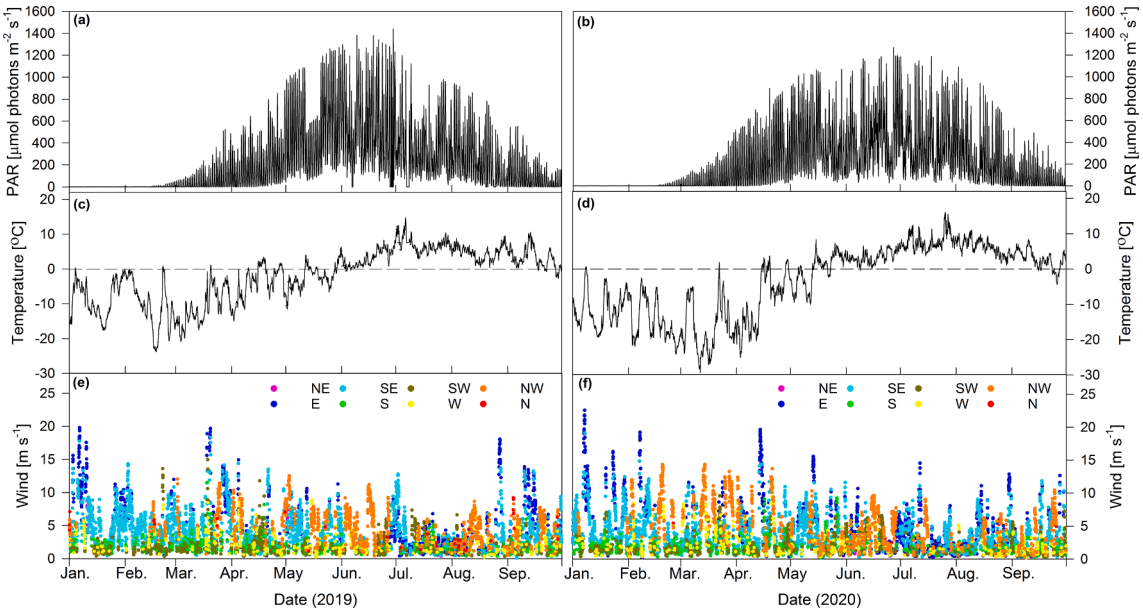

Fig. 2. Atmospheric forcing during 2019 (left) and 2020 (right): a, b) hourly-averaged incoming PAR (µmol photons m^{-2} s^{-1}), c, d) air temperature (°C), e, f) wind speed (m s^{-1}) and direction.

April 2020. Commonly, northwesterly winds are recorded in Ny-Ålesund only when the larger-scale synoptic wind is from the same direction. Synoptic wind coming from any other direction will always be subject to local effects by the heterogeneous surface structure. These local effects include wind channeling due to orography determined by the mountains surrounding Kongsfjorden and cold air drainage caused by cooling over the Holtedahlfonna glacier field. As a result, near-surface wind with speed > 5 m s^{-1} generally occurs parallel to the fjord axis, predominantly from east-southeasterly direction and less frequently from northwest (Beine et al., 2001; Maturilli et al., 2013), as also apparent in the blue and orange peaks shown in Fig. 2 e, f.

3.2. Sea ice conditions

The sea-ice conditions in Kongsfjorden differed markedly between spring 2019 and 2020 (Fig. 3). In 2019, fast-ice in Kongsfjorden lasted only until April and was restricted to the inner, shallower parts of Kongsfjorden while in 2020 it lasted until June and extended past Ny-Ålesund (Table 2; see also Fig. S1). In 2019, the sea ice conditions in Kongsfjorden were similar to other recent years (e.g. 2013, 2015, 2017 and 2018), while 2020 was more exceptional and in the range of years prior to 2006 and the cold years from 2009 to 2011 (Pavlova et al. 2019; Gerland et al., 2020). In 2020, the first pelagic sampling with MS *Teisten*

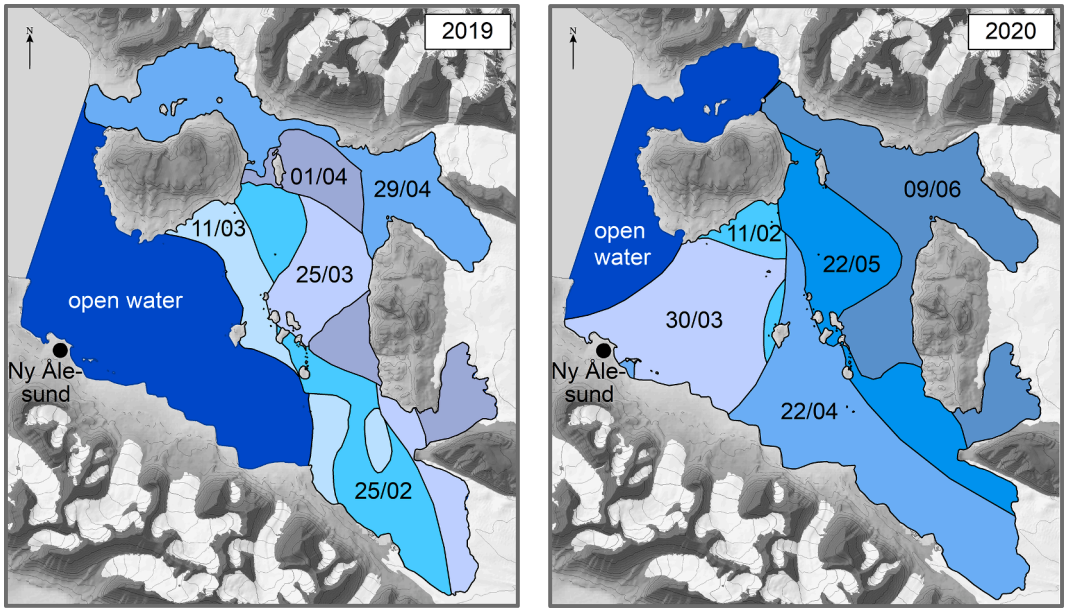

Fig. 3. Sea-ice extent in Kongsfjorden for 2019 (left panel) and 2020 (right panel). Different colors correspond to sea-ice extent on respective dates, and open water (dark blue) is also indicated (following the color scheme used in Pavlova et al., 2019). The Ny-Ålesund Research Station is indicated with a black dot. (For interpretation of the references to color in this figure legend, the reader is referred to the web version of this article.)

Table 2
Maximum fast-ice coverage in Kongsfjorden (in % of observational area) for each month from February to June in 2019 and 2020.

Year	February	March	April	May	June
2019	47.3	54.1	18.3	–	–
2020	64.6	87.4	88.1	48.1	30.7

had to be postponed until 1 May due to drifting sea ice outside Ny-Ålesund. The more heavy ice condition was further supported by more extensive drift ice on the shelf west of Spitsbergen in spring 2020 compared to ice-free conditions at the same time in 2019 (Fig. S2).

3.3. Water masses

The mooring data from winter to summer showed higher subsurface water temperature and salinity in 2019 (Fig. 4a) than in 2020 (Fig. 4b), and consequently the presence of different water masses in the two years. The dominance of TAW and AW in spring and summer indicate a more advective regime in 2019, while the presence of colder Local Water (LW) and Winter Cooled Water (WCW) indicate a more local regime in 2020 (Fig. 4). The water mass time-series in 2020 (Fig. 4b) showed the Atlantic-origin water masses only by the first week of June, below Intermediate Water (IW) that was present up to nearly 25 m in the water column. Following the delineations by Tverberg et al. (2019), the presence of TAW over the subsurface water column in January, generally less sea ice, and AW found during summer at shallower depths indicated 2019 as a "Winter Open" scenario (Fig. S3). On the other hand, 2020 was a "Winter Deep" scenario with limited episodic Atlantic water advections below 100 m in January and February and summer advection at intermediate depths (Fig. S3).

3.4. Water mass characteristics

Water temperatures in spring differed markedly between the two years (Fig. 5a, b). Spring water temperatures in 2019 were > 1 °C throughout the upper 250 m of the water column (only upper 150 m shown in Fig. 5a, b) while spring water temperatures in 2020 did not exceed 0 °C. In both years, surface warming commenced in early June with water temperatures of up to 8 °C in the upper 60 m by early August. A decrease in the surface layer salinity started to develop in June in both years leading to a 10–30 m low salinity surface layer that can be attributed to land and glacier meltwater run-off (Fig. 5c, d). The freshening was more pronounced in 2020 than in 2019, found at 17 m depth in the second week of July and strengthening by the end of August (Fig. 4b). The MLD was deep (150 m) in spring 2019 while it was shallow in spring 2020 except one wind mixing event down to 100 m in late May (Fig. 5a, b). In both years, MLD shoaled by early June at depths of generally < 30 m coincident with surface warming and meltwater run-off. The turbidity increased by 2 to 5 times in June over the same depth range as that of the fresher surface water layer (Fig. 5e, f).

The spring bloom, as depicted by *in situ* Chl *a* fluorescence profiles (Fig. 5g, h), lasted from roughly mid-May in both years to late June in 2019 and early June in 2020. Maximum Chl *a* concentrations from discrete samples reached 12.9 μg L^{-1} at 25 m on 3 June 2019 and 10.5 μg L^{-1} at 5 m on 22 May 2020. With a few exceptions chl *a* concentrations did not exceed 2 μg L^{-1} during the summer (Table 3), but were generally higher in summer 2019 than in summer 2020 (Fig. 5g, h). The euphotic zone depth shoaled (up to 4 m) during the spring bloom periods and continued to shoal during the summer months as a result of the high turbidity from meltwater runoff. Nitrate and silicic acid concentrations during the early bloom phase (late April 2019 and early May 2020) in the upper 25 m (Table 3) were similar but lower than values measured at mid-fjord location in winter 2014 (9.8–11 μM nitrate and 4–4.9 μM silicic acid; Hegseth et al., 2019). However, nitrate concentrations during

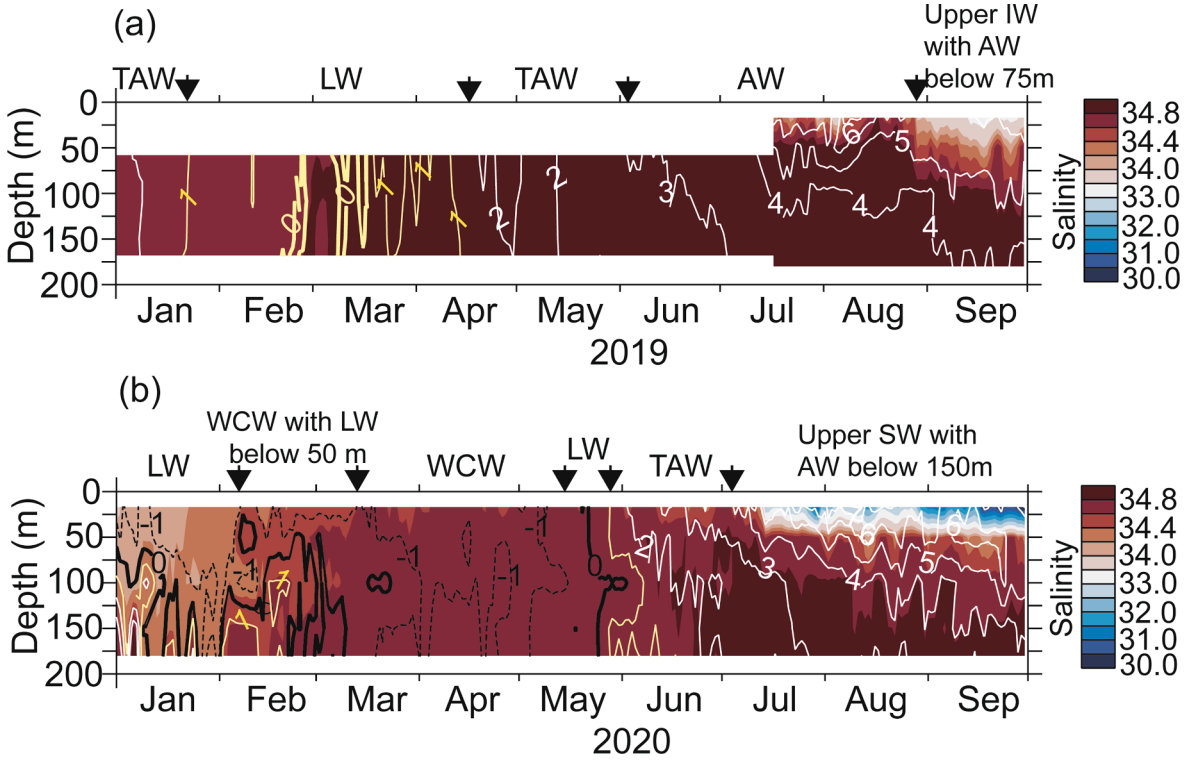

Fig. 4. Water mass properties prior to and during the plankton sampling period for 2019 (a) and 2020 (b), as measured from the IndARC mooring: salinity in shades overlaid by temperature (°C) in contours. The shift in the presence of water masses over time is marked with arrows. Water mass type abbreviations: SW, Surface Water; IW, Intermediate Water; AW, Atlantic Water; TAW Transformed Atlantic Water; WCW, Winter Cooled Water; LW, Local Water. Water masses were classified according to Cottier et al. (2005).

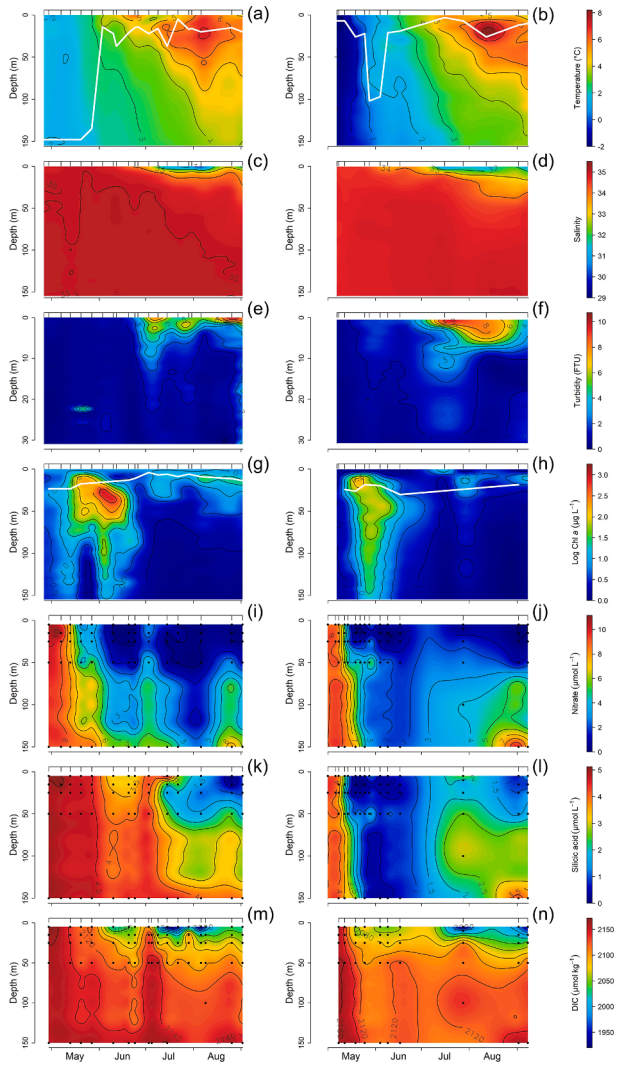

Fig. 5. Water column characteristics at Kb3 in Kongsfjorden in 2019 (left column) and 2020 (right column): a, b) water temperature including mixed layer depth (white line), c, d) salinity (S), e, f) turbidity (FTU), g, h) calibrated Chl *a* fluorescence including 1% PAR depth (white line), i, j) nitrate, k, l) silicic acid and m, n) dissolved inorganic carbon (DIC). Sampling occasions are marked with tick labels. Temperature, salinity, Chl *a* fluorescence and FTU are measured from CTD casts. Sampling depths of discrete nutrient and DIC measurements are marked with black dots. Note that Chl *a* is given in logarithmic scale and turbidity is only shown for the upper 30 m.

the early bloom phase 26 April to 7 May 2019 were significantly higher than during the early bloom phase 1 to 8 May 2020 (Student *t*-test, $p = 0.00006$). The decline in nitrate (Fig. 5i, j) and particular silicic acid (Fig. 5 k, l) was more rapid in 2020 as compared to 2019. Subsurface (>5 m) silicic acid concentrations remained elevated in 2019 until late July (>2.7 µmol L^{-1}) while nitrate concentrations in the upper 50 m were < 0.6 µmol L^{-1} throughout the summer of both years. The seasonal trend in DIC generally followed the ones for nitrate and silicic acid with initial DIC drawdown coinciding with the spring bloom and a low DIC surface layer developing in summer (Fig. 5m, n). In 2019, the decline was largest in the upper 50 m and extended down to 150 m while in 2020 the DIC decline extended deeper to about 225 m.

3.5. Seasonal trends in protists carbon biomass and nutrients

Depth-integrated Chl *a* standing stocks peaked at > 300 mg m^{-2} in early June 2019 and mid-May 2020 (Fig. 6a, b). The increase and collapse of the bloom was steeper in 2020 than in 2019, while the 2019 spring bloom lasted roughly 2 weeks longer. Summer Chl *a* standing stocks were higher in 2019 than in 2020. Based on monthly climatology of satellite-derived Chl *a* for Svalbard waters, the spring bloom on the adjacent West Spitsbergen shelf and eastern Fram Strait occurred in June, in both years, with a more pronounced bloom in 2019 than in 2020 (Fig. S4). The protist carbon (PC) standing stocks, based on microscopic cell counts, followed the Chl *a* stocks with a few exceptions when heterotrophic protists dominated the biomass (see further details below). The same applied for depth-integrated POC and PON standing stocks (Fig. 6c, d) with the exception of the high POC and PON standing stocks in late July 2020. In both years, ratios of POC:Chl *a* (g:g) and POC:PON (mol:mol) dropped from > 200 and > 6 during the pre-bloom phase to values of < 100 and < 6 during the bloom phase (Table 3), which is indicative of a community shift towards autotrophic dominance and a decline in the detrital fraction. During the summer months (see Table 1), the POC:Chl *a* ratio (g:g) was on average 389 ± 111 (2019) and 345 ± 173 (2020) and the POC:PON ratio (mol:mol) 5.5 ± 1.2 (2019) and 4.5 ± 0.2 (2020). Note that only subsurface depths of 25 and 50 m were taken to derive the ratios in 2020 due to the high sediment content in surface waters. Nitrate inventories integrated over the upper 50 m of the water column largely decreased by early June 2019 and mid-May 2020 due to consumption by the spring bloom (Fig. 6e, f). Smaller peaks in nitrate, as well as silicic acid, were observed in early July 2019 and late May and mid-June 2020 (Fig. 6e, f). In 2020, the silicic acid inventory followed the decline in nitrate while it only showed a gradual decrease in 2019 and never fell below 100 mmol m^{-2}. Interestingly, elevated nitrate and particularly silicic acid inventories were measured during the sampling event in late July 2020, which coincided with the massive tidewater glacier run-off event (Fig. S5). In 2019, the decline in the DIC inventory was more gradual as compared to the nitrate drawdown while in 2020 the DIC inventory during the bloom period followed a similar rapid decline as nitrate and silicic acid (Fig. 6g, h). Detailed information on bloom stages and respective light and mixed layer characteristics can be found in Table 1.

3.6. Carbon drawdown and export

We estimated the DIC loss or gain (ΔDIC) in the upper 50 m of the water column relative to a winter value of 2158 µmol kg^{-1} and normalized to a salinity of 35 based on average winter values at Kb3 estimated by Fransson et al. (2016). A positive ΔDIC value denotes a gain of DIC relative to the winter value, and a negative value corresponds to a loss in DIC. The maximum depth-integrated ΔDIC in the upper 50 m showed a loss of 62 g C m^{-2} for the period 29 April to 24 June 2019 and a loss of 44 g C m^{-2} for the period 8 May to 4 June 2020 (Fig. 7a, b). These correspond to daily losses of 1 and 1.9 g C m^{-2} d^{-1} during the bloom periods in 2019 and 2020, respectively.

The seasonal evolution of the deep water ΔDIC was estimated at 300 m depth (Fig. 7c, d) and showed large differences between the two years. The maximum excess DIC of about 28 µmol C kg^{-1} was similar in both years, but the timing and rate of gain were different. In 2019 values were initially relatively low, and reached maximum values at the end of summer whereas in 2020, the maximum excess DIC was observed during the spring bloom and decreased rapidly. In 2020, the ΔDIC values were more than twice as low at the end of summer than at the same time in 2019.

3.7. Protist diversity, standing stocks and community composition

In total 176 protist taxa were identified during the seasonal sampling in 2019 and 2020. The actual number of species is higher since this estimate includes flagellates differentiated into size groups and some taxa were only identified to genus level. The total number of identified taxa at any one date varied between 34 and 74 and was comparable between the two years (Fig. 8a, b). Diatoms, dinoflagellates and other

Table 3
Nutrient concentrations (NO_3, $Si(OH)_4$ and PO_4 (μmol L^{-1})), discrete Chl *a* measurements (μg L^{-1}), particulate organic carbon (POC) and nitrogen (PON), Protist Carbon (PC), POC:Chl *a* (C:Chl *a*) ratio and POC:PON (C:N) ratio collected at station Kb3 in Kongsfjorden in 2019 and 2020. Samples are listed according to sampling dates and depths. Asterisk (*) designates nutrient samples analyzed at the Institute of Marine Research, all other nutrient samples were analyzed at the Alfred Wegener Institute.

Date	Depth [m]	NO_3 [μmol L^{-1}]	$Si(OH)_4$ [μmol L^{-1}]	PO_4 [μmol L^{-1}]	Chl a [μg L^{-1}]	POC [μmol L^{-1}]	PON [μmol L^{-1}]	PC [μg L^{-1}]	C:Chla [g:g]	C:N [mol:mol]
26.04.19	5	9.2	4.7	0.4	0.4	8.3	1.0	24.4	235.2	8.5
	15	10.0	4.8	0.4	0.6	5.3	0.9	21.6	101.8	5.7
	25	10.1	4.8	0.4	0.4	22.7	2.3	13.5	775.7	10.0
	50	10.3	5.0	0.5	0.3	8.1	0.8	10.4	283.6	10.3
29.04.19	5	10.8	5.1	0.4	0.0	1.8	0.3	1.4	535.7	5.4
	15	10.5	4.9	0.4	0.2	2.6	0.4	3.4	158.3	6.0
	25	10.2	4.8	0.4	0.5	3.9	0.8	20.3	88.3	5.2
	50	9.9	4.9	0.4	0.6	2.8	0.6	12.3	61.6	4.6
07.05.19	25	9.1	4.7	0.4	0.7	5.7	0.6	27.5	103.2	8.9
	50	9.0	4.7	0.4	0.7	4.6	0.7	28.1	78.0	6.4
13.05.19	5	7.2	4.8	0.4	2.9	15.4	2.8	59.4	63.3	5.4
	15	7.2	4.7	0.4	2.8	15.3	2.8	NA	64.8	5.4
	25	7.3	4.7	0.4	2.5	14.4	2.7	NA	68.9	5.3
	50	7.7	4.7	0.4	2.0	9.1	1.7	32.6	54.7	5.2
20.05.19	5	2.5	4.6	0.3	6.5	27.8	4.9	141.2	51.1	5.7
	15	3.8	4.7	0.3	6.2	23.6	4.2	141.2	45.5	5.7
	25	4.0	4.7	0.3	6.1	22.5	4.1	NA	44.0	5.5
	50	4.1	4.7	0.3	6.7	19.6	3.3	77.2	35.0	5.9
27.05.19	5	3.7	4.5	0.3	3.4	17.6	3.2	44.4	62.8	5.6
	15	3.3	4.5	0.3	5.7	21.7	4.0	82.1	46.0	5.5
	25	3.6	4.5	0.3	6.7	21.8	3.9	124.7	39.0	5.5
	50	5.3	4.6	0.3	3.0	14.9	2.5	67.0	58.8	5.9
03.06.19	5	0.0	3.8	0.1	1.8	17.5	2.8	40.8	118.5	6.2
	15	0.0	4.1	0.1	4.3	36.1	4.8	98.3	101.9	7.5
	25	0.0	4.3	0.2	12.9	55.4	7.5	192.3	51.6	7.4
	50	3.0	4.4	0.3	8.2	28.1	5.0	340.6	41.3	5.6
10.06.19	5	0.0	3.2	0.1	1.1	15.0	2.0	18.1	163.3	7.6
	15	0.0	3.3	0.1	1.1	23.4	4.3	28.5	262.8	5.5
	25	0.0	3.6	0.1	5.8	38.9	5.7	25.1	80.3	6.8
	50	1.1	3.8	0.2	7.5	35.3	5.5	96.7	56.4	6.4
20.06.19	5	0.0	3.1	0.1	0.6	10.5	1.9	17.5	215.0	5.5
	15	0.0	3.3	0.1	1.1	11.2	2.1	14.6	117.8	5.4
	25	0.0	3.4	0.1	1.6	15.9	2.9	22.7	115.9	5.6
	50	1.2	4.0	0.2	3.0	18.9	3.0	56.0	75.4	6.4
24.06.19	5	0.0	3.1	0.1	0.3	9.4	1.9	21.2	355.2	5.0
	15	0.0	3.3	0.1	0.4	11.0	2.0	26.3	344.1	5.5
	25	0.0	3.5	0.1	0.4	8.3	1.4	16.0	285.3	5.8
	50	0.0	3.8	0.1	0.4	13.3	2.0	37.2	421.6	6.6
03.07.19	5	2.3	4.1	0.2	0.3	9.5	1.3	5.7	412.2	7.3
	15	2.4	4.2	0.3	0.3	10.4	2.3	12.7	461.0	4.5
	25	1.6	4.1	0.2	0.4	9.2	1.7	25.7	289.1	5.4
	50	3.8	4.4	0.3	0.2	8.8	1.6	34.7	728.8	5.4
09.07.19	5	1.5	4.1	0.2	2.6	4.1	0.9	73.7	18.7	4.6
	15	0.0	2.2	0.1	2.0	3.6	0.8	51.0	22.2	4.7
	25	0.0	2.5	0.1	1.5	2.5	0.6	40.5	19.7	4.4
	50	5.5	4.1	0.4	0.1	1.9	0.5	10.5	232.1	4.2
15.07.19	5	1.6	4.9	0.2	1.0	13.4	2.5	41.9	164.4	5.5
	15	0.0	2.1	0.1	1.0	13.0	2.4	88.0	160.4	5.3
	25	0.0	1.7	0.1	1.1	12.2	2.2	92.7	129.1	5.5
	50	0.4	2.6	0.2	0.3	5.3	1.2	54.5	187.4	4.5
22.07.19	5	0.0	2.8	0.1	2.6	20.4	4.0	64.2	96.1	5.2
	15	0.5	2.5	0.1	1.1	10.4	2.0	52.9	109.2	5.2
	25	0.0	2.0	0.1	0.7	10.9	2.1	64.5	198.9	5.3
	50	0.0	1.9	0.1	0.2	5.0	1.0	33.3	263.4	4.9
29.07.19	5	1.0	3.4	0.2	0.8	9.2	1.5	0.7	147.0	6.2
	15	0.0	1.7	0.1	0.4	8.6	1.3	20.8	250.7	6.8
	25	0.0	1.7	0.1	0.2	5.0	0.7	17.6	368.1	7.6
	50	0.5	2.3	0.2	0.2	7.3	0.9	33.1	466.2	8.6
06.08.19	5	0.0	1.7	0.0	1.5	17.8	3.3	32.6	142.3	5.5
	15	0.0	1.5	0.0	1.7	30.8	4.2	65.5	217.2	7.3
	25	0.0	1.1	0.1	0.5	7.0	1.3	43.3	168.2	5.4
	50	0.0	1.6	0.1	0.2	5.2	1.0	38.4	262.8	5.4
09.08.19*	5	1.3	3.1	0.2	0.1	3.5	1.0	NA	692.9	3.5
	15	0.7	1.5	0.2	0.6	9,34	1.7	NA	200.3	5.4
	25	0.6	1.8	0.2	0.0	9,38	1.6	NA	3786.6	6.0
	50	1.5	2.2	0.3	0.2	12.8	2.1	NA	1039.5	6.1
26.08.19	5	0.0	0.1	0.0	3.1	18.6	3.1	65.6	73.0	6.0
	15	0.0	0.3	0.1	2.3	14.6	2.4	70.6	77.7	6.2
	25	0.0	1.1	0.1	1.7	10.2	1.9	50.0	73.1	5.3
	50	2.4	2.4	0.2	0.7	4.4	0.8	38.6	76.3	5.4
02.09.19	5	0.0	0.9	0.1	0.8	26.9	5.4	37.5	411.0	5.0

(*continued on next page*)

Table 3 (*continued*)

Date	Depth [m]	NO_3 [µmol L^{-1}]	$Si(OH)_4$ [µmol L^{-1}]	PO_4 [µmol L^{-1}]	Chl a [µg L^{-1}]	POC [µmol L^{-1}]	PON [µmol L^{-1}]	PC [µg L^{-1}]	C:Chla [g:g]	C:N [mol:mol]
	15	0.0	0.8	0.1	1.8	12.6	2.5	72.0	85.6	5.0
	25	0.0	0.9	0.1	0.9	10.3	1.7	28.0	139.8	6.1
	50	0.9	1.7	0.2	0.4	5.4	1.0	31.9	147.0	5.6
01.05.20	5	8.3	4.1	0.5	1.2	NA	NA	28.4	NA	NA
	25	9.2	4.3	0.5	0.6	NA	NA	37.4	NA	NA
06.05.20	5	8.1	4.0	0.5	0.5	NA	NA	21.2	NA	NA
	25	8.7	4.0	0.6	0.2	NA	NA	50.4	NA	NA
08.05.20	5	8.4	3.9	0.5	0.6	33.7	6.9	56.1	730.0	4.9
	15	8.4	3.9	0.5	0.4	5.8	0.8	73.3	192.5	7.5
	25	8.9	4.0	0.5	0.3	3.0	0.7	16.4	132.0	4.4
	50	8.9	4.0	0.5	0.2	3.6	0.6	8.9	194.6	5.9
12.05.20	5	5.4	2.9	0.3	3.5	20.0	3.3	138.0	67.8	6.0
	15	5.3	2.2	0.3	3.6	18.7	2.9	116.6	63.3	6.4
	25	6.6	2.0	0.4	3.3	15.7	2.3	107.1	57.9	6.9
	50	8.9	3.8	0.5	0.4	6.6	0.8	40.1	193.4	7.9
14.05.20	5	1.6	1.1	0.2	3.0	NA	NA	146.6	NA	NA
	25	0.9	0.6	0.2	2.1	NA	NA	60.4	NA	NA
19.05.20	5	0.0	0.1	0.1	3.4	26.7	3.6	220.1	94.2	7.5
	15	0.0	0.1	0.1	5.6	46.4	5.6	191.5	99.2	8.3
	25	0.4	0.1	0.1	7.2	28.4	4.5	177.9	47.6	6.3
	50	3.8	0.8	0.3	4.7	NA	NA	294.0	NA	NA
22.05.20	5	0.9	0.5	0.2	10.5	NA	NA	188.1	NA	NA
	25	1.7	0.6	0.2	6.1	NA	NA	253.0	NA	NA
	50	5.5	1.6	0.4	5.4	NA	NA	237.3	NA	NA
25.05.20	5	0.4	0.3	0.1	6.3	30.8	5.1	231.7	58.5	6.0
	15	0.0	0.1	0.1	4.1	36.2	5.7	144.0	105.6	6.3
	25	1.0	0.4	0.1	5.4	27.9	5.0	93.6	62.7	5.6
	50	1.7	0.6	0.2	3.4	19.7	3.4	102.0	70.2	5.7
28.05.20	5	2.7	1.4	0.2	4.4	NA	NA	NA	NA	NA
	25	2.9	0.8	0.3	3.6	NA	NA	NA	NA	NA
	50	6.1	1.8	0.4	3.4	NA	NA	NA	NA	NA
04.06.20	5	0.1	0.3	0.1	0.4	15.5	2.8	43.7	485.6	5.6
	15	0.0	0.3	0.1	1.7	27.9	4.7	122.3	194.2	5.9
	25	0.6	0.5	0.3	2.8	22.8	4.2	57.8	96.7	5.5
	50	1.9	0.6	0.3	2.6	22.2	3.7	55.0	102.2	6.0
09.06.20	5	0.8	0.5	0.2	0.4	17.2	3.2	120.5	493.9	5.4
	15	0.0	0.3	0.1	1.3	22.5	4.2	229.6	202.5	5.4
	25	0.2	0.4	0.1	0.9	14.1	2.7	51.9	199.9	5.3
	50	2.4	1.1	0.3	4.3	18.1	3.1	46.5	50.8	5.9
17.06.20	5	0.8	0.7	0.2	0.4	11.8	2.0	29.9	374.7	5.8
	15	0.2	0.5	0.2	0.3	12.3	2.0	37.3	438.6	6.3
	25	0.6	0.4	0.2	0.3	8.9	1.1	26.6	343.4	7.9
	50	1.4	0.9	0.3	0.8	10.6	2.0	23.2	164.7	5.5
28.07.20*	5	0.6	2.8	0.1	0.1	42.2	12.8	0	5220.2	3.3
	15	0.3	1.6	0.1	0.1	20.7	5.5	0	1719.6	3.8
	25	1.7	1.9	0.3	0.3	12.7	3.0	0.5	467.2	4.3
	50	2.6	2.5	0.4	0.5	9.9	2.1	2.0	222.4	4.6
02.09.20	5	0.0	0.7	0.1	0.3	16.5	2.9	79.8	643.2	5.7
	15	0.0	0.9	0.1	0.9	11.2	2.1	61.1	157.8	5.3
	25	0.0	1.0	0.1	0.4	4.4	1.0	8.5	153.0	4.4
	50	0.9	1.4	0.2	0.1	4.8	0.8	6.7	640.9	5.9
08.09.20	5	0.1	1.7	0.1	1.6	17.1	3.0	46.0	132.2	5.7
	15	0.0	0.7	0.1	0.9	9.9	1.9	47.1	131.7	5.2
	25	0.3	1.5	0.2	0.3	4.3	0.8	6.8	194.3	5.5
	50	1.7	1.8	0.3	0.1	3.2	0.8	7.3	546.8	4.1

flagellates were the groups with highest species richness, while for ciliates generally < 10 species were identified (Fig. 8c-j). The lowest number of species was recorded in late July 2020 coincident with high turbidity. The Shannon diversity and Pielou's evenness indices were similar for both years, with minimum values during the spring blooms and higher during the early bloom period and summer (Fig. 8k, l). During the *P. pouchetii*-dominated bloom in 2019, the Shannon and Pielou's indices were lower than during the diatom-dominated bloom in 2020.

Total PC standing stocks peaked at 9 g C m^{-2} and 11.5 g C m^{-2} in early June 2019 and late May 2020, respectively (Fig. 9a, b). In 2019, the spring bloom was dominated by *P. pouchetii* while in 2020 diatoms dominated, succeeded by *P. pouchetii*. Both diatoms and *P. pouchetii* were minor components of the PC standing stocks during the summer, though for diatoms, a small bloom was observed in late summer 2019. Ciliate standing stocks peaked in May and early June but remained at low levels throughout the rest of the summer, when flagellates showed peak values. Dinoflagellate standing stocks were rather constant throughout the observational period, with some minor peaks in spring and mid-summer 2019.

In 2019, diatom standing stocks did not exceed 0.2 g C m^{-2} throughout the season, except for the late summer bloom of 1.2 g C m^{-2}. In contrast diatoms peaked at 8.6 g C m^{-2} in early June 2020 but remained at levels < 0.1 g C m^{-2} throughout the remainder of the summer (Fig. 9c, d). Diatoms were dominated by centric species in both years, while pennate species contributed significantly only in early May. In 2019, the late summer bloom was dominated by *Chatoceros* spp., *Rhizosolenia* spp. and *Thalassiosira* spp., while in 2020, the spring bloom assemblage was dominated by the centric diatoms *Thalassiosira hyalina*, *T.* cf. *gravida/antarctica* var. *borealis* and *T. nordenskioeldii*. These species

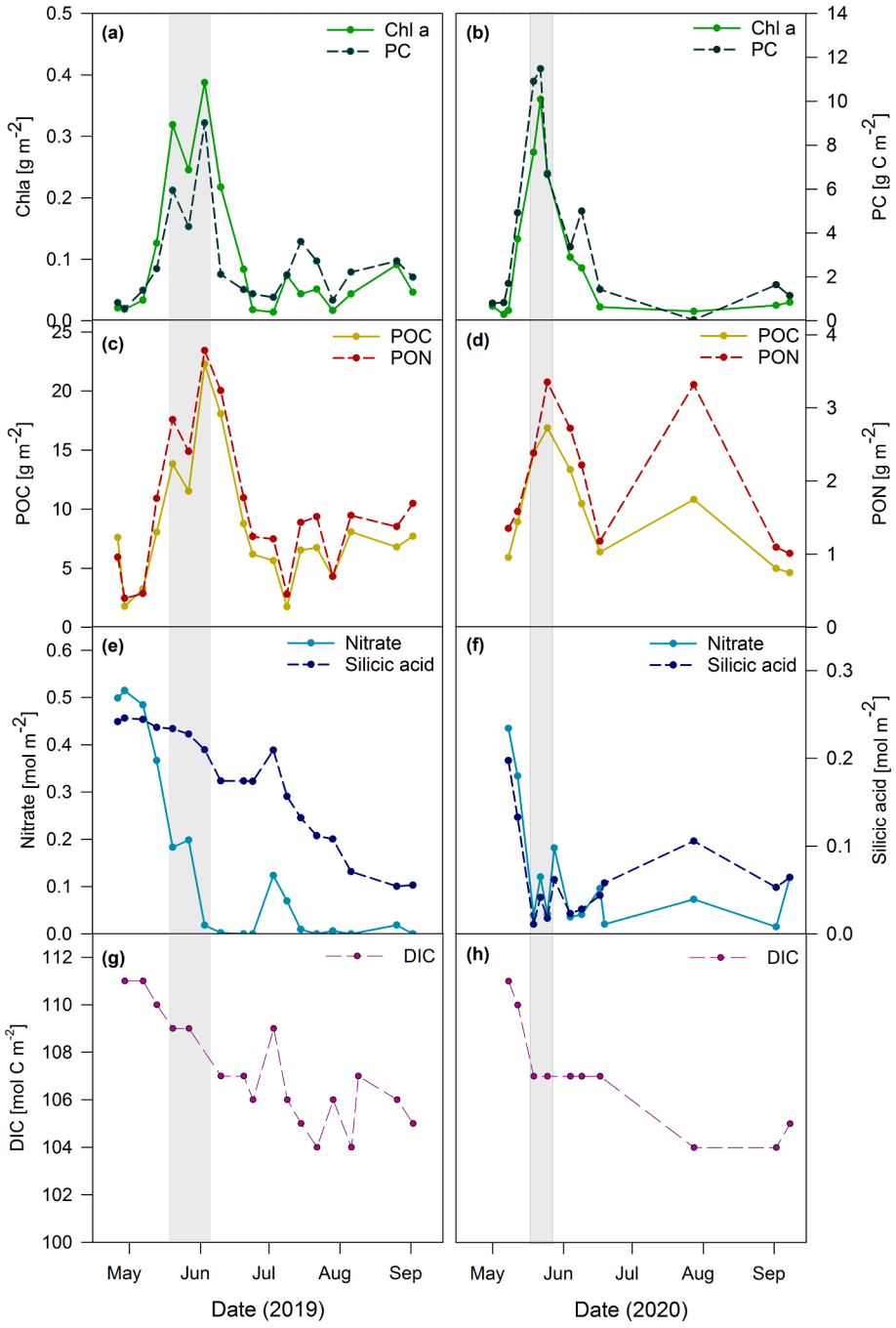

Fig. 6. Depth-integrated standing stocks/inventories (0–50 m) in 2019 (left) and 2020 (right): a, b) Chl *a* and protist carbon (PC), c, d) POC and PON, e, f) nitrate (NO_3) and silicic acid ($Si(OH)_4$, and g, h) dissolved inorganic carbon (DIC). The respective peak bloom periods are shaded in gray.

combined, contributed to 85% and 47% of diatom and PC standing stocks in spring 2020, respectively. Accumulation rates of *T. hyalina*, *T.* cf. *gravida/antarctica* var. *borealis* and *T. nordenskioeldii* were 0.08, 0.08 and 0.12 d^{-1}, respectively, during the muted diatom increase in spring 2019 while they were 0.1, 0.14 and 0.33 d^{-1} during the increase phase of the bloom in 2020. *Porosira glacialis* and *Eucampia groenlandica* were among the co-dominant species during the peak of the bloom in 2020.

The haptophyte *Phaeocystis pouchetii* was by far the single-most dominant species during the 2019 spring bloom and co-dominant in the 2020 spring bloom, following in succession after the diatoms (Fig. 9e, f). In both years, the colonial form of *P. pouchetii* dominated biomass with nearly identical peak standing stocks of 6.2 and 6.1 g C m^{-2} and similar timing. In summer, *P. pouchetii* standing stocks remained < 0.2 g C m^{-2} and solitary cells were the prevalent form. Accumulation rates of *P. pouchetii* during the spring bloom build-up phase were 0.22 and 0.3 d^{-1} in 2019 and 2020, respectively.

Strombidium spp. dominated ciliate standing stocks during both spring blooms. In mid-June 2020, a peak standing stock of 2.9 g C m^{-2} coincided with the collapse of the *Phaeocystis* bloom (Fig. 9g, h). The mixotrophic ciliate *Mesodinium rubrum* accounted for a considerable fraction of ciliate standing stocks at some sampling occasions, particularly during the spring bloom in 2019. Tintinnid ciliates (*Parafavella obtusangula*, *Ptychocylis obtusa*, *Tintinnopsis* spp.) contributed a minor share to ciliate standing stocks during both years.

With a few exceptions, unarmored (athecate) dinoflagellates dominated over armored (thecate) dinoflagellates (Fig. 9i, j). Within the

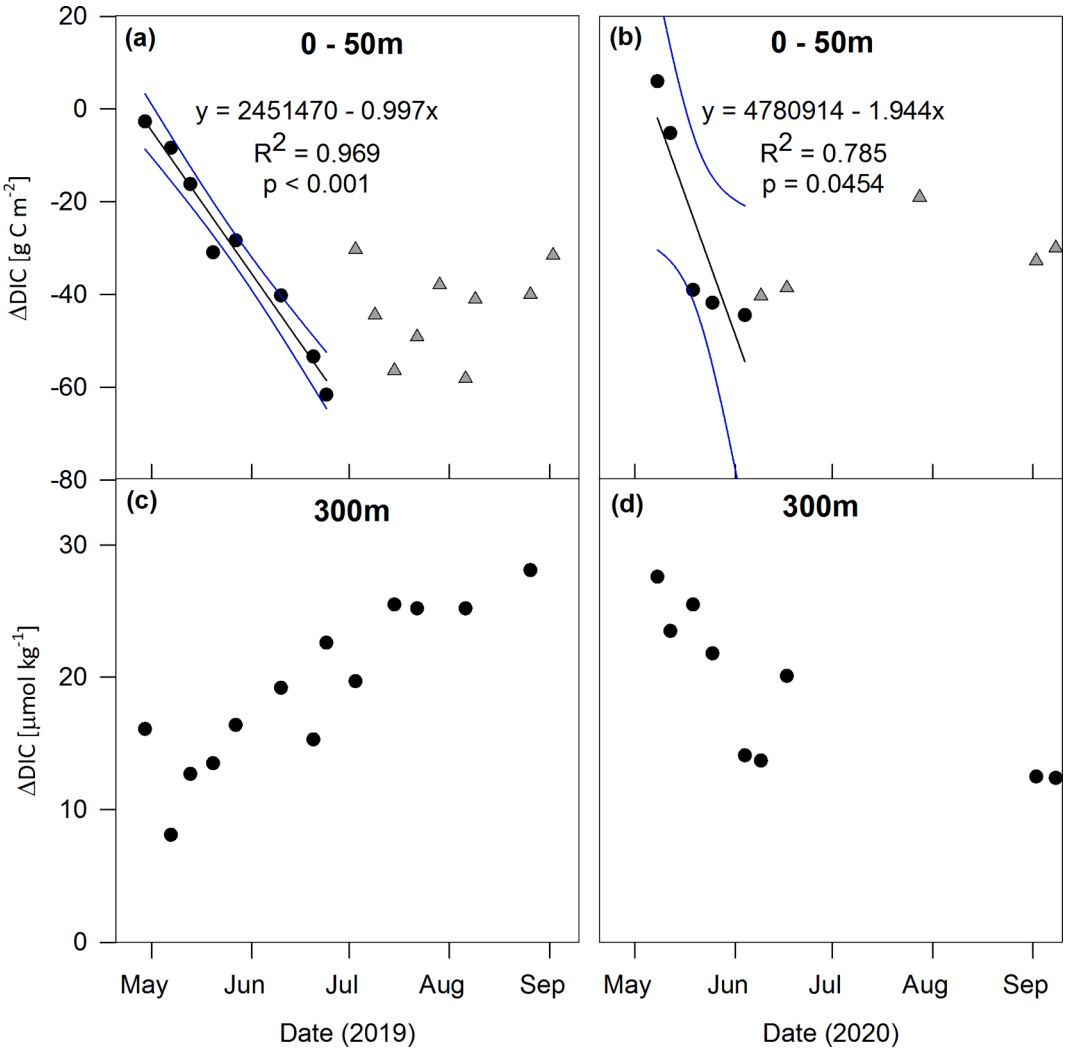

Fig. 7. Depth-integrated (0–50 m) DIC change in g C m^{-2} relative to winter values for 2019 (a) and 2020 (b). A negative value denotes a loss of DIC. The linear regression and 95% confidence interval are only plotted for the respective bloom periods (black dots) and the summer period indicated with another symbol (gray triangle). The seasonal evolution of the deep water DIC change at 300 m depth in 2019 (c) and 2020 (d).

athecate dinoflagellates, species of the genus *Gymnodinium*, largely represented by *G.* cf. *arcticum*, *G.* cf. *gracilentum*, *G.* cf. *galeatum* and *G.* cf. *wulffii*, co-dominated dinoflagellate standing stocks, followed by *Gyrodinium fusiforme*. The thecate dinoflagellate *Heterocapsa* cf. *niei* was a prominent component of the dinoflagellate assemblage in early spring 2019 while species of the pallium-feeding genus *Protoperidinium* (*P. pellucidum*, *P. pallidum* and *Protoperidinium* sp.) accounted for a considerable fraction of dinoflagellate biomass during the late-summer diatom bloom in 2019 and the spring bloom in 2020. The large peak of other dinoflagellates in early May 2020 was mainly due to dinoflagellate cysts.

Flagellate (size range 2–20 µm) standing stocks for the period May and June were higher in 2019 than in 2020, while they were comparable in early September (Fig. 9k, l). The dominant flagellate taxa were the cryptophyte *Cryptomonas* sp., the dictyochophyte *Pseudopedinella pyriformis*, the chlorophyte *Pterosperma* sp. and the choanoflagellate *Calliacantha natans*. *Cryptomonas* sp. and *Pterosperma* sp. contributed to a smaller bloom in July 2019 also reflected in elevated Chl *a* standing stocks during that time (Fig. 6a).

3.8. Zooplankton standing stocks and community composition

A total of 74 zooplankton taxa were identified during the 2019 and 2020 seasons, covering a size range from small mesozooplankton to macrozooplankton. Results are presented with taxa sorted according to size (small and large copepods, macrozooplankton) and planktic life history (meroplankton versus holoplankton) (Fig. 10). Zooplankton dry mass (g DM m^{-2}) peaked at 41 g m^{-2} in early August 2019 and at 39 g m^{-2} in late July 2020, and was dominated by large copepods of the genus *Calanus* in both years (Fig. 10a, b). During the bloom period in 2020, meroplankton co-dominated the zooplankton biomass. Small copepods never contributed >9.2% in 2019 and 13.8% in 2020 to total summer zooplankton biomass. However, they were a numerically dominant component of the zooplankton community during summer. Macrozooplankton including krill (euphausiids), arrow worms (chaetognaths) and amphipods (*Themisto* spp.) were minor contributions to zooplankton standing stocks in this study.

Standing stocks of large copepods were dominated by *Calanus finmarchicus* and *C. glacialis* (Fg. 10c, d). *Calanus finmarchicus* peaked at 28 g m^{-2} in early August 2019 and 19 g m^{-2} in late July 2020 while *C. glacialis* peaked in early August 2019 and 2020 with 13 and 16 g m^{-2}, respectively. The ratio of *C. finmarchicus* to *C. glacialis* was quite variable between sampling dates in 2019 with a tendency towards *C. finmarchicus* dominance in that year, while *C. glacialis* tended to be more dominant in 2020. The next two most important species, *C. hyperboreus* and *Metridia longa*, never exceeded 17% of large copepod standing stocks.

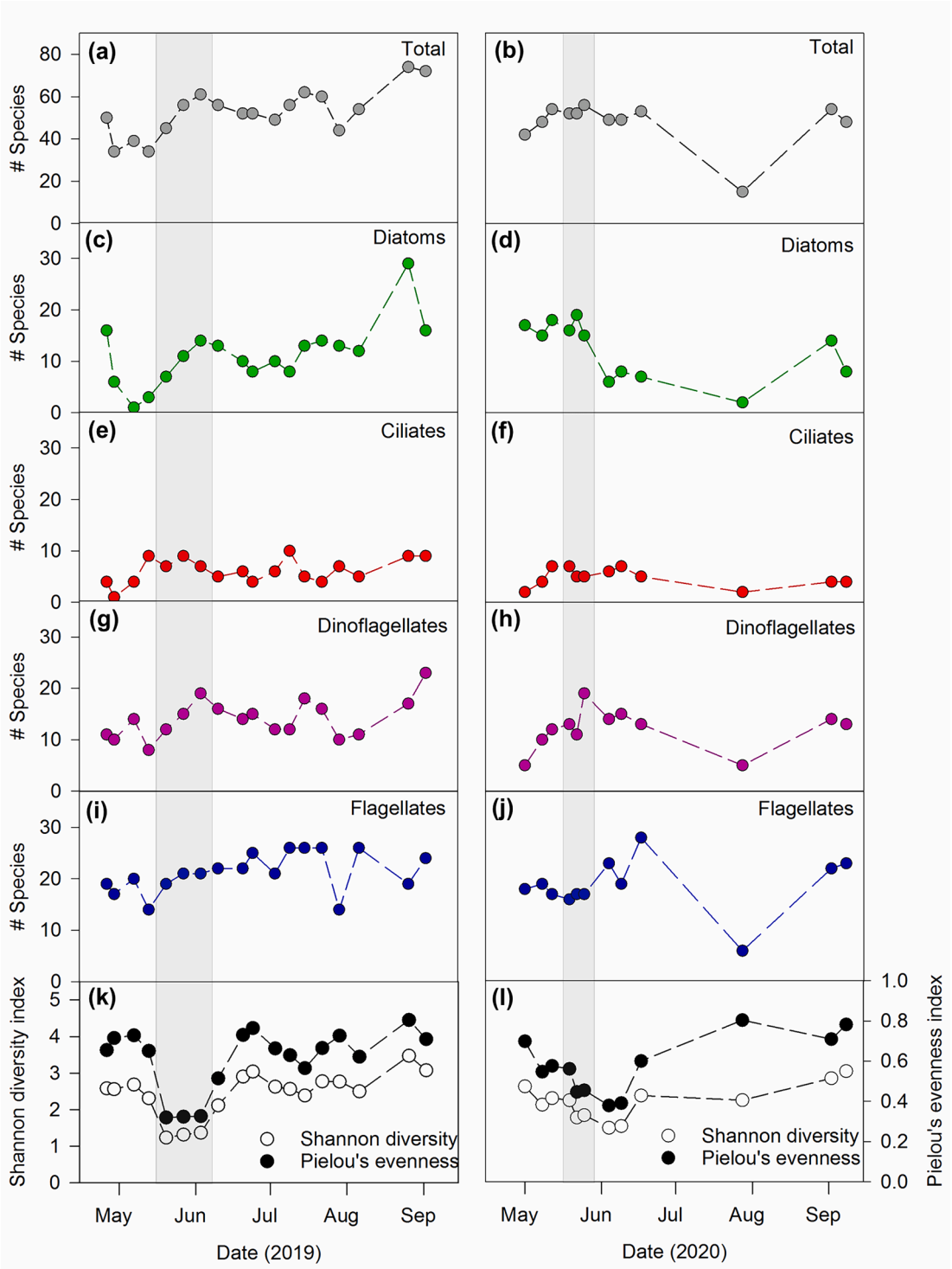

Fig. 8. Total protist (a,b), diatom (c,d), ciliate (e,f), dinoflagellate (g,h), flagellate (i,j) species richness and Shannon diversity and Pielou evenness indices (k,l) for the upper 50 m. The peak bloom periods are shaded in gray.

Oithona spp. and *Pseudocalanus* spp. showed seasonal increases and dominated the small copepod standing stocks during late summer (Fig. 10e, f). *Microcalanus* spp. and *Acartia* spp. contributed minor fractions to small copepod standing stocks. Copepod nauplii dominated in spring and early summer, particularly in 2020 and were largely represented by nauplii of *Calanus*.

In spring, meroplankton standing stocks showed marked differences between the years. In spring 2019 meroplankton was only recorded at one sampling occasion, with 0.2 g C m^{-2}, while in early June 2020 peak standing stocks of 3.7 g C m^{-2} rivaled those of large copepods (Fig. 10g, h). Cirripedia nauplii dominated meroplankton standing stocks in spring during both years, while Bivalvia veligers dominated in early August 2019. Echinodermata larvae, Polychaeta larvae and Gastropoda veligers were minor contributors to meroplankton standing stocks.

Macrozooplankton standing stocks remained below 2.5 g m^{-2} during both years (Fig. 10i, j). Krill dominated during the pre-bloom period in 2019, while chaetognaths dominated prior to the bloom in 2020. Euphausiid larvae and juveniles showed a pronounced increase in May-

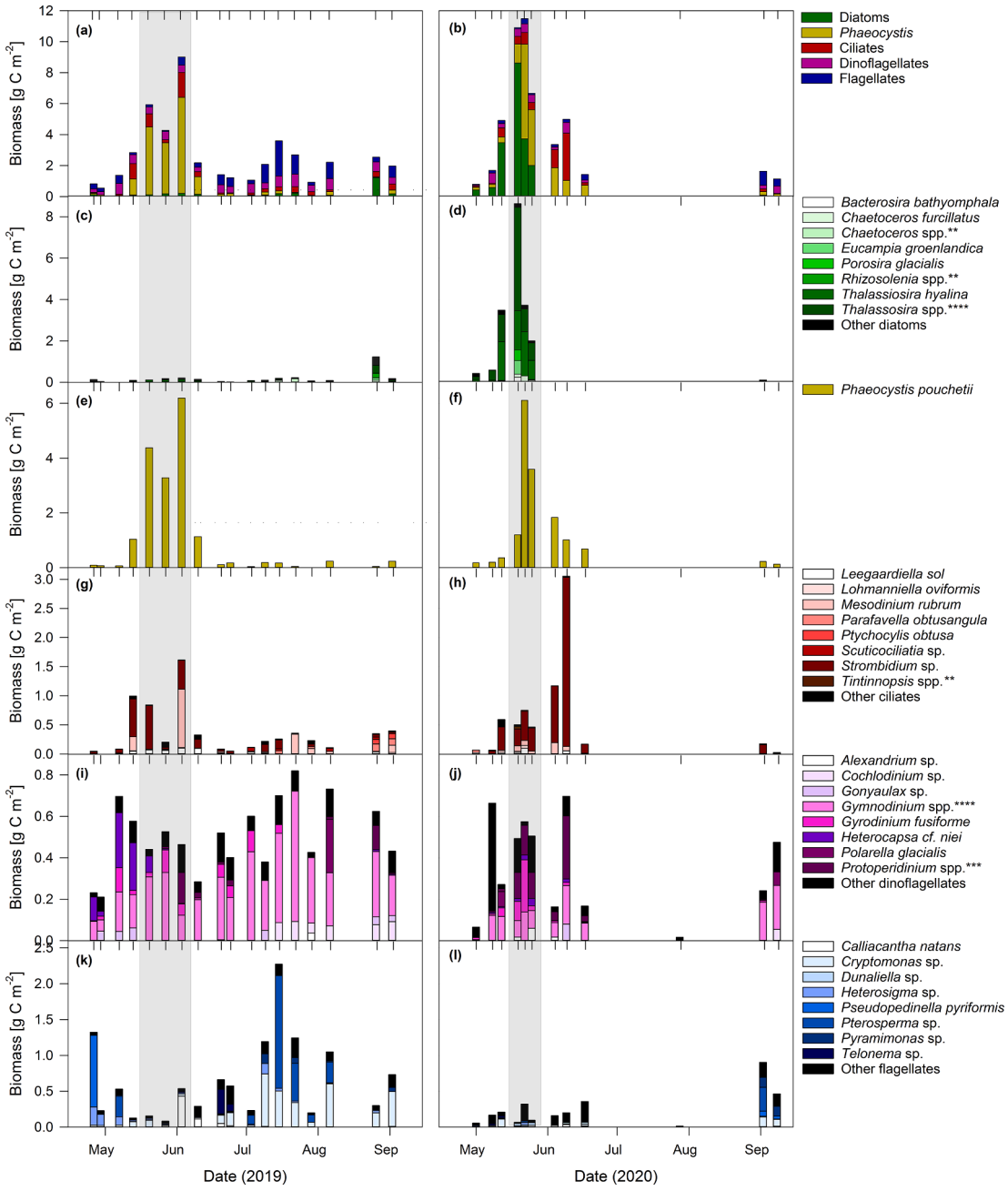

Fig. 9. Depth-integrated standing stocks (0–50 m) of the dominant protist groups and taxa. The peak bloom periods are shaded in gray. The number of stars represents the number of species behind some of the genera and is detailed in the following: *Chaetoceros* spp.** *(C. decipiens, C. laciniosus), Rhizosolenia* spp.** *(R. borealis, R. hebetata), Thalassiosira* spp.*** *(T. gravida, T. antarctica var. borealis, T. nordenskioeldii), Tintinnopsis* spp.** *(T. beroidea, Tintinnopsis* sp.*), Gymnodinium* spp.*** *(G.* cf. *gracilentum, G.* cf. *galeatum, G.* cf. *wulffii), Protoperidinium* spp.*** *(P. pellucidum, P. pallidum, Protoperidinium* sp.*).*

June 2020 coinciding with the spring bloom, while their seasonal increase was less pronounced in 2019 and showed a larger temporal off-set to the bloom. In August and early September 2019, the shell-bearing pteropod (winged-snail) *Limacina helicina* and the hyperiid amphipods *Themisto abyssorum* and *T. libellula* dominated macrozooplankton. In late July and early September 2020, *L. helicina* was also an important macrozooplankton species. In early September 2020, another pteropod, *Clione limacina*, also made an equally large contribution to the macrozooplankton stock.

3.9. *Calanus and microzooplankton grazers relative to the spring bloom*

To assess the recruitment of the two dominant *Calanus* species, *C. finmarchicus* and *C. glacialis,* we looked specifically at the timing of copepodid stages CI-CV, adult females (AF) and adult males (AM) relative to the spring bloom expressed as Chl *a* standing stock. In both years, and for both species, the increase in copepodids CI-CIII abundance followed the spring bloom with an approximately two to three week delay depending on the copepodid stage while copepodid CIV and CV abundance increased during the decline phase of the bloom (Fig. 11). However, the abundance of early copepodids CI-CIII were up to an order of magnitude lower during spring 2019 (when the bloom was *Phaeocystis*-dominated and drawn in time and peaked later) than during spring 2020 (when the bloom was diatom-dominated and more concentrated and peaked earlier), particularly for copepodid stages CI and CII. CIVs were also more abundant in 2020 than 2019 for both species. Despite the

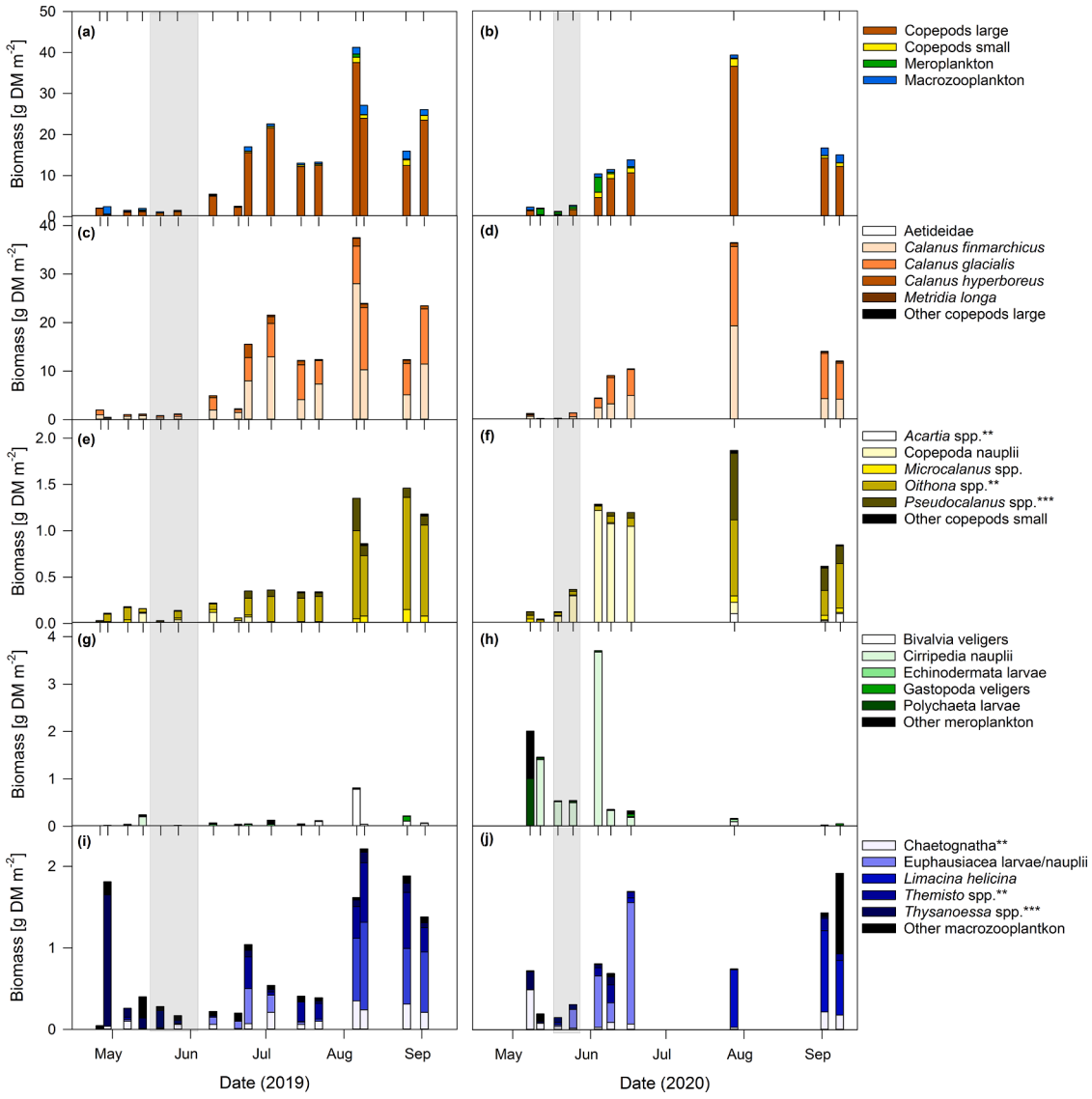

Fig. 10. Depth-integrated standing stocks (0–300 m) of the dominant zooplankton groups and taxa. The peak blooms periods are shaded in gray. The number of stars represent the number of species behind some of the genera and are detailed in the following: *Acartia* spp.** *(A. longermis, A. clausi), Oithona* spp.** *(O. similis, O. atlantica), Pseudocalanus* spp.*** *(P. acuspes, P. minutus, P. moultoni),* Chaetognatha *(Eukrohnia hamata, Parasagitta elegans), Themisto* spp.** *(T. abyssorum, T. libellula), Thysanoessa* spp.*** *(T. inermis, T. raschii, T. longicaudata).*

apparent better recruitment (to CIV) in 2020, the copepodids CV of *C. glacialis* and *C. finmarchicus* peaked at similar levels in late summer in both years, and were even slightly higher in 2019. During the spring bloom period (early to end of May), AF of *C. finmarchicus* had significantly higher abundances in 2019 than in 2020 (Student *t*-test, p = 0.,046). For the remainder of the season, the abundance of AF of both species stayed low with the exception of a smaller peak of *C. finmarchicus* and *C. glacialis* in early July 2019 while in 2020 AF increased during the months of June and July in both species (Fig. S6). Adult males of *C. finmarchicus* were only observed in April and May 2019 and May and early June 2020, and in very low abundances while males of *C. glacialis* were not found in either year (Fig. S6).

We zoomed into ciliates, dinoflagellates and the dominant phytoplankton taxa during the spring bloom phases in 2019 and 2020 in order to get a better impression of the potential role of microzooplankton grazing (Fig. 12). *Phaeocystis pouchetii* had similar abundances in both years while the bloom-forming diatoms *Thalassiosira hyalina*, *T. nordenskioeldii* and *T. antarctica* var. *borealis* had 66, 63 and 33-fold higher abundances during the bloom period in 2020 (Fig. 12 a-d). Ciliate abundances were similar during the bloom phase of both years while dinoflagellates had 3.1-fold higher abundances in 2019 (Fig. 12 e, f). The higher abundance of dinoflagellates in 2019 is not reflected in standing stocks (Fig. 9 i) as smaller *Gymnodinium* taxa dominated relative to the spring bloom in 2020 when large *Protoperidinium* species and *Gyrodinium fusiforme* dominated (Fig. 9 j).

Although correlation between two variables does not necessarily signify a trophic relationship as could be achieved via stable isotope or lipid biomarker analysis (see e.g. Kohlbach et al. 2021), the Spearman rank correlation matrix provides an indication of potential trophic relationships within the plankton community, especially if embedded within an ecological context. The generally fewer significant relationships in 2020, despite a number of high correlation coefficients (>0.6), can be explained by the fewer data points for the spring bloom period than in 2019. The protist community was more top-down controlled (negative correlations) by zooplankton grazers in 2020 than in 2019, with the exception of *Phaeocystis* and flagellates (Fig. 13). Especially diatoms and dinoflagellates showed negative relationships with most of the zooplankton grazer groups for the spring bloom period 2020.

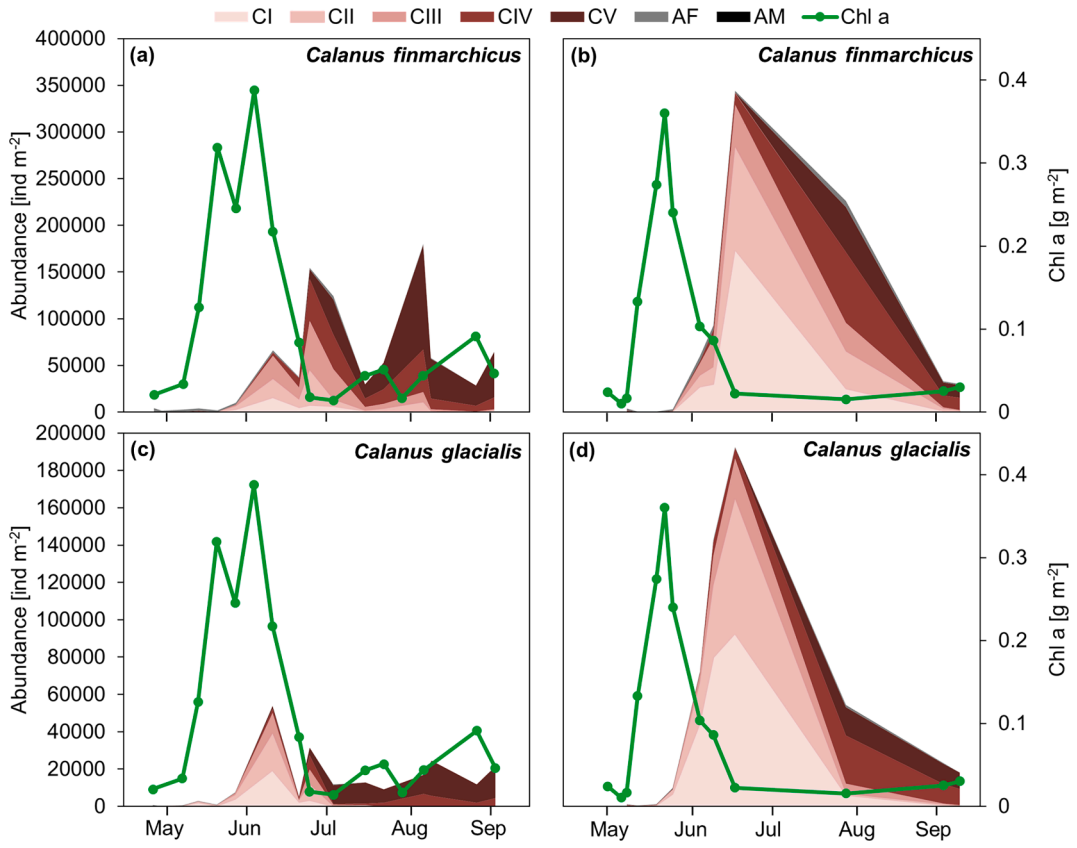

Fig. 11. Depth-integrated Chl *a* standing stocks (mg m^{-2}; 0–100 m) and cumulative abundance (ind. m^{-2}) of *Calanus finmarchicus* (a, b) and *C. glacialis* (c, d) copepodid stages CI-CV, adult females (AF) and adult males (AM) in 2019 (left column) and 2020 (right column).

Flagellates on the other hand were negatively correlated with the other protist groups in 2020. The strong positive correlation within the zooplankton community during the spring bloom in 2020, with the exception of meroplankton, suggests a common driving factor while the correlations of different signs in 2019 suggests a more complex pattern.

4. Discussion

4.1. Environmental setting

The years 2019 and 2020 were characterized by contrasting hydrographical regimes illustrated by the marked differences in water mass properties. The dominance of TAW in January and from mid-April onwards in 2019 points to advection of AW from the WSC into the fjord. This "Winter Open" scenario (Tverberg et al., 2019) allows for advection of AW into Kongsfjorden during winter and spring. Conversely, the presence of LW and WCW during winter and spring 2020 is indicative of a "Winter Deep" scenario (Tverberg et al., 2019), a setting not favorable for advection of AW into the fjord. This together with colder air temperatures in late winter and spring 2020 facilitated a more extensive and longer lasting sea-ice cover than in any year since 2011 (Pavlova et al., 2019). Furthermore, a period of relatively persistent and strong northwesterly winds from February to early April 2020 also contributed to keeping sea ice within the fjord which is consistent with the maximum sea-ice extent at the end of March and a reduction thereafter. Although northwesterly winds are a prerequisite for AW advection into the fjord (Cottier et al., 2005), the relatively long period of northwesterly winds in February and March 2020 does not seem to have led to much advection of AW into the fjord. Probably the strong density gradient between the colder and fresher local fjord waters and AW provided an effective barrier at the fjord mouth for AW to enter the fjord as proposed by Cottier et al. (2005). The water masses inside the fjord in winter and spring 2019 were more similar to AW, thus the conditions were more favorable for advection in that year.

The difference in the timing of northwesterly winds likely also had a strong impact on the wind mixing regime of the surface water column. Winds from a northwesterly direction are representative of the larger synoptic wind field with much larger wind fetch resulting in more effective wind mixing of the surface water column compared to easterly-southeasterly winds blowing from the glacier field along the fjord axis. Thus, the coincidence of northwesterly winds with the spring bloom in 2019 can explain the more deeply wind-mixed conditions as compared to 2020 when northwesterly winds ceased in early April.

The summers were characterized by meltwater run-off from land, a typical feature of glaciated arctic fjords. Starting in June, a thin (<10 m), fresher, relatively warm (2–4 °C) and turbid surface layer developed in both years, coinciding with air temperatures rising above 0 °C and starting meltwater run-off. The high turbidity is due to high suspended mineral matter loads associated with surface and subglacial meltwater run-off from land- and marine-terminating glaciers lining the coastline of Kongsfjorden (Halbach et al., 2019; Bhaskar et al., 2023). Apart from its negative impact on the subsurface light field, the high turbidity also contributed to warming of the surface layer by absorbing more solar radiation. The sampling in late July 2020 coincided with a heatwave on Svalbard (air temperatures > 20 °C in Longyearbyen) and massive run-off from the marine-terminating glaciers in inner Kongsfjorden (Fig. S5). This is also reflected in the more pronounced low salinity surface layer in summer 2020 compared to summer 2019 (Fig. 4). The year 2020 was one of three years with the highest annual marine heatwave intensity and duration for the Barents Sea area, including Svalbard, in the time period from 1982 to 2020 (Mohamed et al. 2022). Interestingly, the run-off event in late July 2020 coincided with elevated surface silicic acid concentrations which are likely linked to glacier meltwater which has been shown to be an important source of silicic acid to fjord systems in

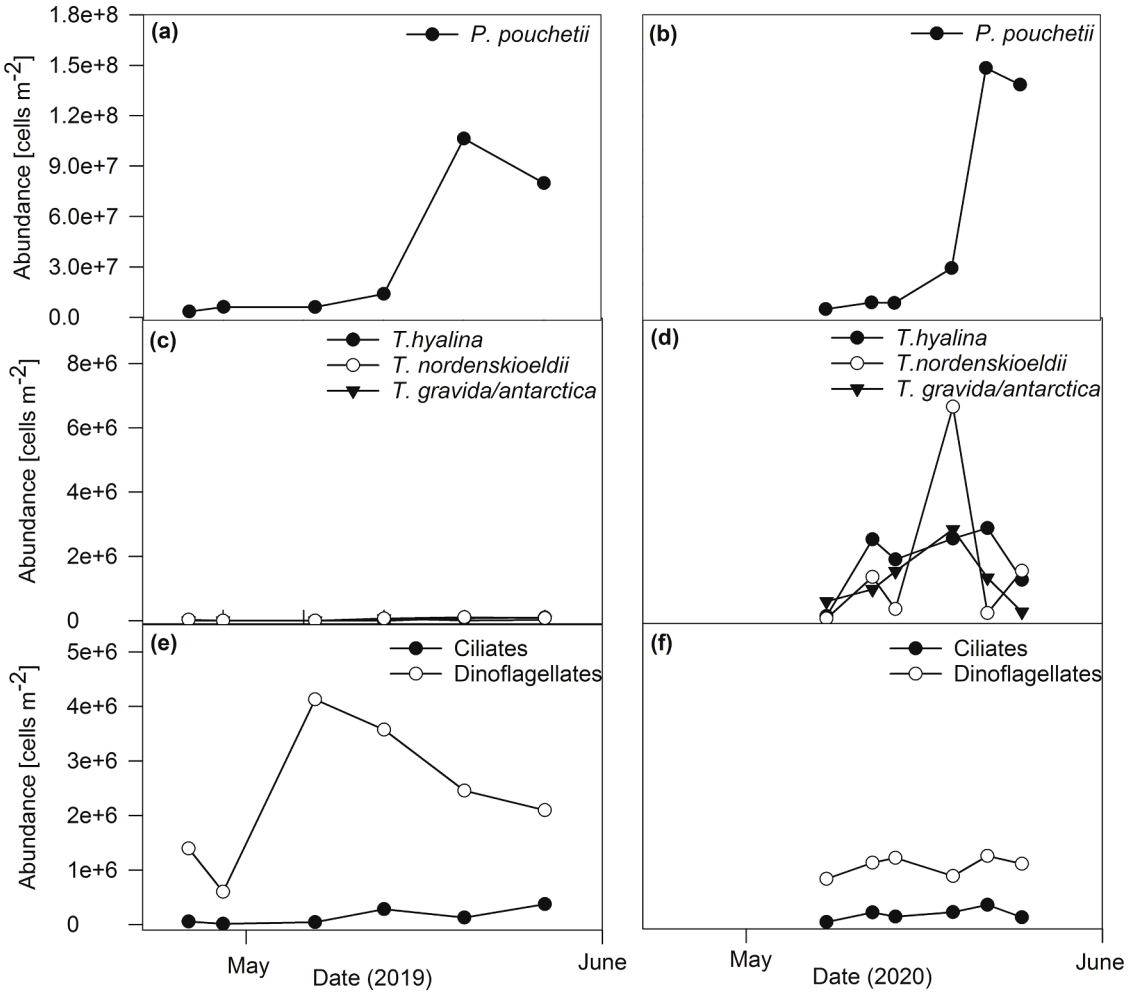

Fig. 12. Depth-integrated abundance of *Phaeocystis pouchetii* (a, b), *Thalassiosira hyalina*, *T. antarctica* var. *borealis* and *T. nordenskioeldii* (c, d), ciliates and dinoflagellates (e, f) (cells m^{-2}) in 2019 (left column) and 2020 (right column).

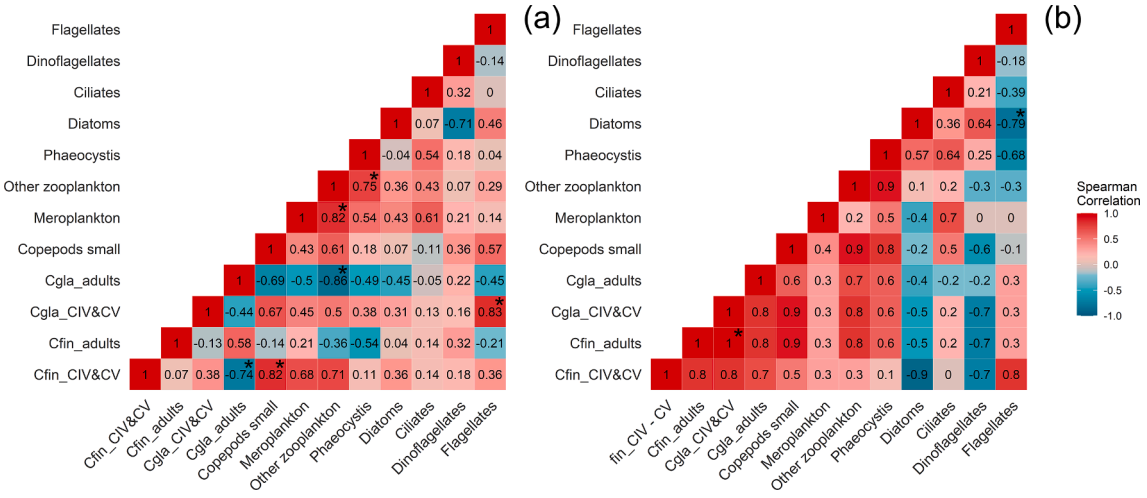

Fig. 13. Spearman rank correlation matrix for major protist and zooplankton groups for the spring bloom period in 2019 (a) and 2020 (b). Values show the Spearman rank results (significant correlations of $p < 0.05$ are marked with an asterisk). Red colors show positive correlations, blue colors show negative correlations. Cgla_adults = *Calanus glacialis* adults (both females and males), Cgla_CIV&CV = *C. glacialis* copepodid stages CIV and CV, Cfin_adults = *Calanus finmarchicus* adults (both females and males), Cfin_CIV&CV = *C. finmarchicus* copepodid stages CIV and CV. (For interpretation of the references to color in this figure legend, the reader is referred to the web version of this article.)

Greenland (Meire et al., 2016) and Svalbard (Halbach et al., 2019; Vonnahme et al., 2021). Furthermore, the high POC and PON stocks coincident with the massive sediment run-off event could be explained by high loads of particle-bound organic carbon and nitrogen. The high sediment concentrations also obscured microscopic cell counts, explaining the very low PC stocks in late July 2020 and the mis-match with the Chl *a* stocks on that date.

4.2. Mechanisms determining spring bloom dominance

Both years were characterized by sizable spring blooms of $>$ 8 g PC m^{-2} and $>$ 300 mg Chl *a* m^{-2}, comparable to values reported from previous studies in Kongsfjorden (Hegseth et al., 2019). A striking contrast between 2019 and 2020 was the difference in the composition of the phytoplankton spring bloom. In 2019, the phytoplankton community was strongly dominated by the colonial stage of the haptophyte *Phaeocystis pouchetii* for the entire spring bloom period, while in 2020 the spring bloom initially was dominated by diatoms of the genus *Thalassiosira* and then succeeded by *P. pouchetii*. Both *Phaeocystis* and diatoms are well known to dominate spring bloom phytoplankton assemblages in temperate to polar coastal waters (Degerlund and Eilertsen, 2010; Hegseth et al., 2019), and similar contrasting patterns in spring bloom community composition during successive years have been reported from Adventfjorden, another Atlantic-influenced fjord in Svalbard (Dabrowska et al., 2021). However, the mechanisms determining species dominance during bloom periods are poorly understood. Improving our understanding of the underlying controls of bloom dominance is important to elucidate the wider food web and biogeochemical implications, as the fate of bloom biomass is strongly influenced by its species composition (Smetacek et al., 2004; Assmy et al., 2013). Phytoplankton blooms are a function of inoculum size and integrated growth rates of species' populations in the surface mixed layer on the one hand, and of their loss rates via sinking and mortality on the other. The growth environment is determined by bottom-up factors (temperature, light and nutrients) while the mortality environment is regulated by top-down factors (pathogens, parasites, and grazers). In the following we will discuss the role of bottom-up and top-down factors in determining the bloom dominance patterns we observed in two years of contrasting environmental conditions.

The blooms we observed in Kongsfjorden represent local processes and are unlikely to have been advected from outside the fjord. The satellite-derived Chl *a* monthly climatologies suggest that the spring bloom on the adjacent West Spitsbergen shelf and eastern Fram Strait started later in June in both years, similar to what has been seen in other studies (Hegseth et al., 2019; Lampe et al. 2021). One would expect more abrupt changes in spring bloom composition and biomass if advective processes would have dominated. Indeed, TAW was the dominant water mass throughout the spring bloom period in 2019 and in 2020 a shift from LW and WCW dominance to TAW dominance only happened in early June when the bloom already declined, suggesting that changes in water masses were unlikely to have impacted bloom patterns and composition.

The euphotic zone depth in spring did not differ markedly between the two years. However, phytoplankton cells suspended in the surface mixed layer would have experienced lower average light levels in 2019 due to the generally deeper surface mixed layer in spring 2019 compared to the more stratified water column in spring 2020. Winter-replenished nutrient concentrations in early spring were well above limiting concentrations in both years and their availability is unlikely to have impacted the observed dominance patterns during the early phase of the spring bloom. However, the significantly higher nitrate concentrations during the early bloom phase 2019 than the early bloom phase 2020 sustained an overall larger bloom reflected in the ca 30% higher carbon drawdown during the 2019 spring bloom than during the 2020 spring bloom. Our data also clearly show that low silicic acid concentrations are not a prerequisite for *Phaeocystis* to bloom as also supported by earlier observations (Peperzak et al., 1998; C.J.M. Hoppe, pers. comm).

Despite the differences in mixed layer depth, the timing of the start of the spring bloom was similar in the two years, suggesting that the spring bloom was not delayed by deeper mixed layers in 2019, which is corroborated by previous studies (Backhaus et al., 2003; Eilertsen et al., 1989; C.J.M. Hoppe, pers. comm). The deeper mixed layers in 2019 resulted in a slower bloom build-up, but longer-lived bloom while the stratified situation in 2020 resulted in a more "pulsed" bloom with a steeper biomass increase and decline. This relationship between euphotic zone depth and mixed layer depth is known to affect the rate of bloom growth (Assmy et al., 2019), reflected in the lower accumulation rates of the bloom-forming *Thalassiosira* species and *Phaeocystis* during the deeply mixed spring 2019 than during the more stratified spring 2020. This is further supported by the negative relationship between mixed layer depth and depth-integrated net primary production for three consecutive spring blooms in Kongsfjorden, illustrating increased light limitation of primary production with increasing mixed layer depth (C.J.M. Hoppe, pers. comm). Previous studies from the Arctic Ocean (Reigstad et al., 2002; Degerlund and Eilertsen, 2010; Assmy et al. 2017), as well as the Southern Ocean (Arrigo et al., 2000), suggest that *Phaeocystis* can outcompete diatoms under low light conditions, which is supported by its dominance during the deeper wind-mixed conditions and its roughly two-fold higher accumulation rates than the *Thalassiosira* species in spring 2019. However, the higher biomass accumulation rates of *P. pouchetii* in spring 2020 likely indicate that it grew faster under stratified than deeply-mixed conditions. In addition, diatoms have been shown to dominate in deeply mixed layers (Backhaus et al., 1999; Smetacek et al., 2012) and *Phaeocystis* in Dutch coastal waters required a higher daily irradiance threshold to bloom than the spring bloom diatoms (Peperzak et al., 1998). In Kongsfjorden, *Thalassiosira*-dominated spring bloom communities exhibited higher primary production rates and more efficient photophysiology than *Phaeocystis*-dominated ones over a range of light intensities (C.J.M. Hoppe, pers. comm), indicating that light-use efficiency is not the cause of *Phaeocystis* dominance under deep wind-mixed conditions. Hence, the poor success of the major bloom-forming diatom species during the 2019 spring bloom, despite their presence, cannot be explained from a bottom-up perspective alone and other factors need to be considered to explain their muted response.

Many spring bloom diatoms are known to form resting spores (von Quillfeldt, 2000; Degerlund and Eilertsen 2010), including the three *Thalassiosira* species dominating bloom biomass in 2020 (von Quillfeldt, 2001) and exhibit a boom and bust life cycle of rapid biomass build-up and decline (Assmy et al., 2019), exemplified by the more pulsed bloom in 2020. Resting spores of bloom-forming diatoms rapidly sink out of the water column towards the end of the bloom (Rey and Skjoldal, 1987; Rynearson et al., 2013), with major implications for the marine carbon cycle (Smetacek, 1985). Surface sediments can be an important source of resting spores for the diatom spring bloom (Eilertsen and Wyatt, 2000; Wiedmann, 2010; Hegseth and Tverberg, 2013; Hegseth et al., 2019). Hence, the life cycle of neritic spore forming diatoms can be regarded as a "space holding" strategy in an otherwise advective pelagic environment. The importance of deep convective mixing in winter for spring bloom inoculation by spore-forming diatoms has been suggested previously (Backhaus et al., 1999; Eilertsen and Wyatt, 2000; Hegseth and Tverberg, 2013; Brown et al., 2015; Hegseth et al., 2019). The "Winter Deep" scenario in 2020 with dominance of local water masses (LW and WCW) in winter and spring 2020 points to deep convective mixing as a mechanism for bottom resuspension of resting spores and could explain the higher abundances of the three *Thalassiosira* species during the early bloom phase in 2020. Although not a prerequisite, the more extensive formation of sea ice in Kongsfjorden in winter and spring 2020 likely facilitated deep convective mixing (Saenko et al., 2002).

Phaeocystis is ubiquitous in the European Arctic, including a wide range of coastal and open ocean settings and water masses around Svalbard (Vader et al., 2015; Metfies et al., 2016; Assmy et al., 2017;

Ardyna et al., 2020; Orkney et al., 2020) and its motile solitary flagellate stage is a dominant component of the protist community in the water column during winter (Vader et al., 2015; Marquardt et al., 2016). Furthermore, a benthic stage dependent on resuspension from the seafloor is not known for *Phaeocystis* (Gaebler-Schwarz et al., 2010; Wiedmann, 2010; Hegseth and Tverberg, 2013), potentially making it less reliant on deep mixing than the spore-forming diatoms. Its ubiquity in Svalbard waters and motile, pelagic lifestyle as a solitary flagellate in winter and early spring (Vader et al., 2015) likely indicate that this species is less dependent on specific water mass characteristics, which would explain similar inoculum abundances during the early bloom phase of both years despite different water mass characteristics.

Grazing by micro- and mesozooplankton grazers is another factor that can shape spring bloom composition and biomass. Adult females of the Atlantic indicator copepod species *Calanus finmarchicus* (Hop et al., 2019b) were significantly more abundant during the early bloom phase in 2019, likely due to more advective AW input, than during the same period in 2020. This is also reflected in the high number of *Calanus* copepod fecal pellets in early May 2019 which were not observed during the same period in 2020 (Fig. S7). Although the higher abundance of *Calanus finmarchicus* and *C. glacialis* AF in early spring 2019 (albeit not significant for the latter species) did not negatively impact eventual bloom biomass build-up, it might have exerted selective grazing pressure on the early spring bloom community. This selectivity can likely be explained by the prey size preferences of the large *Calanus* copepods. The bloom-forming diatoms fall within their preferred prey size range while they cannot make much use of the solitary flagellate stage (ca. 5 μm in diameter) of *Phaeocystis* (Huntely et al., 1987), which is the dominant life stage during the early bloom phase before transitioning into the colonial form. Small size is, thus, an effective size escape in solitary *Phaeocystis* from large copepod grazers (Long et al., 2007). Hence, selective copepod grazing on the bloom-forming diatoms in early spring 2019 may have contributed to the head start of *Phaeocystis* to dominate the bloom in spring 2019.

Ciliates and dinoflagellates are important microzooplankton grazers of phytoplankton in the ocean (Landry and Calbet, 2004) and have been shown to remove a major fraction of daily primary production in temperate to Arctic marine environments (Löder et al., 2011; Lavrentyev et al., 2019). They can respond on the same timescales as their phytoplankton prey, particularly ciliates which are known for their fast reaction times in terms of population growth (Löder et al., 2011), which is illustrated by the marked biomass increases of *Mesodinium rubrum* and *Strombidium* spp. during the bloom periods. Ciliates are important grazers of single *Phaeocystis* cells (Weisse and Scheffel-Möser, 1990; Tang et al., 2001) and *Strombidium* species actively grazed fluorescently-labeled algae which were within the size range of *Phaeocystis* single cells (Archer et al., 2000). The peak in *Strombidium* spp. at the end of the spring bloom in 2020 rivals the highest volumetric microzooplankton biomass reported for the Arctic so far, which was also dominated by *Strombidium* (Lavrentyev et al., 2019). In both years the *Strombidium* spp. peaks coincided with the collapse of *Phaeocystis* indicating that they might have been feeding on the decaying bloom. Indeed, many of the *Phaeocystis* colonies were in a degraded state releasing solitary cells (J. Wiktor person. obs.) which are an accessible prey for large ciliates like *Strombidium* (Peperzak et al., 1998; Archer et al., 2000). Short intense ciliate blooms seem to be a widespread phenomenon (Löder et al., 2012) and are likely quite common but undersampled due to their ephemeral nature. Ciliate grazers may have also impacted the *Phaeocystis* pre-bloom/early bloom inoculum as they could have reduced the abundance of solitary cells before they transitioned into colonial form which provides an effective size escape from ciliates grazers (Long et al. 2007). Solitary *Phaeocystis* cells in the more deeply wind-mixed water column during early spring 2019 could have thus experienced lower encounter rates with ciliate grazers (Behrenfeld, 2010; C.J.M. Hoppe, pers. comm), but the similar abundances of both ciliates and *Phaeocystis* during the bloom phases of both years do not indicate that this was a decisive factor during the two years studied. Ciliates and dinoflagellates generally do not compete for the same phytoplankton prey, as ciliates preferentially graze on phytoplankton < 20 μm while at least the larger dinoflagellates (>20 μm) consume cells that are generally too large for ciliates (Hansen, 1992). Large heterotrophic dinoflagellates of the genera *Protoperidinium* and *Gyrodinium* are able to ingest organisms much larger than themselves (including diatom chains and *Phaeocystis* colonies) through their pallium-feeding and engulf-feeding modes (Jacobson and Anderson, 1986; Stelfox-Widdicombe et al., 2004). Standing stocks of *Protoperidinium* spp. and *Gyrodinium fusiforme* closely matched the diatom spring bloom in 2020 and in case of *Protoperidinium* spp. also the late summer diatom bloom in 2019. Although *Gyrodinium* has been shown to control diatom blooms (Stelfox-Widdicombe et al., 2004; Saito et al., 2006), this is unlikely to have been the case in our study as these large dinoflagellates generally have low growth rates (Jeong and Latz, 1994) relative to their diatom prey (Gilstad and Sakshaug, 1990). Also the higher dinoflagellate abundance during the spring bloom in 2019 (not reflected in biomass) is unlikely to have prevented the diatom bloom as it were largely small *Gymnodinium* species which are not efficient grazers of large spiny diatoms. Large diatom-feeding dinoflagellates on the other hand were conspicuously absent during the spring bloom in 2019 in case of *Protoperidinium* and occurred in lower abundance compared to spring 2020 in case of *Gyrodinium fusiforme*, likely feeding on *Phaeocystis* colonies. Grazing by ciliates and dinoflagellates is unlikely to have controlled the spring bloom in both years, as the large *Phaeocystis* colonies (dominant life stage during the bloom) and the long chains and chitin threads in *Thalassiosira* spp. provide protection against the majority of ciliate and dinoflagellate grazers (Smetacek et al., 2004; Verity et al., 2007; Löder et al., 2012; Lavrentyev et al., 2019). Size escape from microzooplankton grazers as well as top-down control by mesozooplankton (see below) on microzooplankton opens a "loophole" for the large, well-protected phytoplankton taxa to escape the grazer control within the microbial loop and accumulate biomass to bloom proportions (Irigoien et al., 2005).

4.3. Different bloom scenarios and zooplankton recruitment

Our data suggest a better recruitment of copepodids and nauplii of *Calanus* copepods associated with the diatom-dominated spring bloom in 2020. The diatom-dominated bloom had likely channeled more carbon into the classical food chain leading from zooplankton to fish and marine mammals (Haug et al., 2017) than the *Phaeocystis*-dominated spring bloom. This was also revealed by the Spearman rank correlation matrix which showed a generally stronger connectivity between protist groups and zooplankton grazers in 2020 compared to 2019. Despite differences in recruitment success, peak mesozooplankton stocks in late summer were roughly similar in both years, suggesting that advection processes likely outweighed local population growth over an extended period of time. Indeed, the water mass data in summer show advection of AW in both years coinciding with the peak mesozooplankton standing stocks.

In Svalbard coastal waters, cirripedia time their spawning to the spring bloom (Stübner et al., 2016; Søreide et al., 2022). It has been shown that spawning is induced by direct contact with phytoplankton cells (Starr et al., 1991). Although we cannot rule out that we have missed the peak of cirripedia larvae in 2019, as they usually appear during limited periods, the more efficient sinking of the diatom bloom compared to the *Phaeocystis* bloom (see below) likely triggered a larger spawning event in spring 2020. This benthic–pelagic coupling has been shown to drive the patterns of meroplankton composition (Highfield et al., 2010). The fact that also euphausiid larvae showed a better recruitment in 2020 supports the overall better zooplankton recruitment linked to the diatom-dominated compared to the *Phaeocystis*-dominated spring bloom.

4.4. Fate of bloom biomass

The observed POC build-up (22 g C m^{-2} in 2019 and 17 g C m^{-2} in 2020) corresponds to ca. 40% of the DIC drawdown (62 g C m^{-2} in 2019 and 44 g C m^{-2} in 2020), suggesting that ca. 60% of spring bloom production was either eaten or had sunken out of the surface water column. Although top-down control by zooplankton grazing during the bloom in 2019 and particularly in 2020 would have channeled carbon into the marine food web, it is unlikely to have been the main reason for the missing 60% nor the relatively rapid collapse of the blooms. Indeed, copepodids CV of *C. glacialis* likely grazed < 1% protist standing stocks per day during the bloom periods in 2019 and 2020 (based on published ingestion rates for *C. glacialis* CV; Grote et al., 2015). This is likely to have been similar for CV stages of *C. finmarchicus*. During summer, however, *C. glacialis* CV alone could have grazed between 20 and 64% of protist standing stocks per day suggesting a high turnover of the protist community.

Although the overall carbon drawdown in the upper 50 m was greater during the *Phaeocystis*-dominated bloom, the rate of drawdown was about two-fold higher during the diatom-dominated bloom (1.9 g C m^{-2} d^{-1} in 2020 versus 1 g C m^{-2} d^{-1} in 2019) suggesting a more efficient carbon removal, as has been observed previously (C.J.M. Hoppe, pers. comm). We do not have direct measurements of vertical carbon flux but the higher excess DIC at 300 m depth during the peak bloom period in 2020 (23.6 ± 1.9 μmol kg^{-1}) compared to 2019 (14.9 ± 2.0 μmol kg^{-1}) suggests a more efficient export to depth during the diatom spring bloom in 2020, while the gradual seasonal increase of 0.15 μmol DIC kg^{-1} d^{-1} at 300 m in 2019 suggests a rather continuous but low export regime that year. Diatoms and *Phaeocystis* differ with regard to functional traits such as size, morphology, elemental composition, life history, and palatability. These important traits influence how species interact (Lampe et al., 2021), and, critically, how they contribute to the biological carbon pump (Njestgard et al., 2007; Svensen and Vernet, 2016; Wiedmann et al., 2020; Dybwad et al., 2021). Diatoms and particularly the bloom-forming taxa are known to be more efficient in deep carbon export because of their faster sinking rates than *Phaeocystis* (Reigstad and Wassmann, 2007; Wiedmann et al., 2020; Dybwad et al., 2021) while *Phaeocystis* tends to be remineralized in the surface layer unless ballasted by mineral particles (Wollenburg et al., 2018) or deeply mixed (Reigstad and Wassmann, 2007).

4.5. Summer trends in protist and zooplankton communities

The seasonal succession pattern from dominance of bloom-forming diatoms and the colonial stage of *Phaeocystis pouchetii* during the spring bloom towards a more diverse protist community in summer dominated by flagellates and dinoflagellates is a common pattern across a wide latitudinal range, including Svalbard fjords (Kubiszyn et al., 2017: Hegseth et al., 2019). The spring bloom diatoms and *Phaeocystis* realize high growth under nutrient-replete conditions in combination with defense strategies which allow them to escape grazers and accumulate biomass. This is reflected in the highest biomass ratios of autotrophic to heterotrophic/mixotrophic protists during the bloom periods (range from 2 to 11). Thus, the protist community shifted from an autotrophic state in spring to a heterotrophic/mixotrophic state during summer, which is a well-known seasonal feature (Rokkan Iversen and Seuthe, 2011; Kubiszyn et al., 2017; Hegseth et al., 2019). Moreover, POC/Chl *a* ratios dropped from > 100 during the early bloom periods to 35–60 during the bloom periods and subsequently increased again to values > 100 during the summer months.

The spring bloom composition seems to have implications for phytoplankton biomass during the summer season. The higher summer Chl *a* standing stock in 2019 can at least partly be explained by the residual silicic acid not used up during the *Phaeocystis*-dominated spring bloom supporting a late summer diatom bloom. The composition of the late summer bloom was different from the spring bloom, with *Chaetoceros* and *Rhizosolenia* species being co-dominant. Although much smaller in magnitude compared to the spring bloom, late summer/autumn blooms have been reported to be increasing in the Arctic, particularly in the Barents Sea sector (Ardyna et al., 2014; Orkney et al., 2022), and they may also occur in Kongsfjorden (Seuthe et al., 2011; Hegseth et al., 2019). We do not know if they are recurrent annual features, but their contribution to annual production is likely to be relatively small (Dalpadado et al., 2020). Due to the coarser temporal sampling resolution in summer 2020, we might have missed the late summer/autumn bloom in that year.

Copepod grazers exert a strong top-down control on protozoans (Calbet and Saiz, 2005; Löder et al., 2011; Saiz and Calbet, 2011) which is particularly evident for ciliates that show low summer standing stocks when the biomass of large calanoid copepods is at its highest. The peak in *Oithona* spp. in summer can also be linked to their reliance on regenerated production within the microbial food web (Svensen et al., 2019). Small, opportunistic copepod species like *Oithona similis* are part of the retention system and rely on diverse food sources including heterotrophic protists and detritus (Castellani et al., 2005; Rokkan Iversen and Seuthe, 2011). They dominate the zooplankton community in Kongsfjorden in terms of numbers (Hop et al., 2019b) and feed year-round. Selective grazing on ciliates is consistent with previous findings from the Arctic Ocean (Stoecker and Lavrentyev, 2018) and Svalbard fjords (Seuthe et al., 2011; Dabrowska et al., 2021). The elevated flagellate standing stocks during summer compared to spring, on the other hand, indicates trophic cascading effects. Top-down control on ciliates, major grazers of flagellates, by copepods during summer could have released grazing pressure on flagellates. The smaller bloom in July 2019 dominated by *Cryptomonas* sp. and *Pterosperma* sp. could be the result of reduced ciliate grazing pressure and is supported by the dominance of mixotrophic cryptophyte flagellates in Svalbard fjords during the summer (Bae et al., 2022). This is also supported by the negative (2020) or poor (2019) relationship between flagellates and the other protist groups during the spring bloom periods supporting the shift from a diatom and *Phaeocystis*-dominated community in spring to a flagellate-dominated community in summer. Dinoflagellate standing stocks were seasonally more stable, likely as a result of their slower response times and lower susceptibility to zooplankton grazing than ciliates (Löder et al., 2011; Stoecker and Lavrentyev, 2018). Naked dinoflagellates belonging to the genus *Gymnodinium* were a dominant component of dinoflagellate standing stocks in summer. This species-rich but understudied genus (Kubiszyn and Wiktor, 2016) is known to host mixotrophic species (Stoecker and Lavrentyev, 2018). Generally, it needs to be emphasized that the bulk of ciliate and dinoflagellate biomass was dominated by mixotrophic taxa which supports the view that mixotrophy is the dominant nutritional mode in Arctic protist communities, especially in summer (Stoecker and Lavrentyev, 2018). Their flexible nutritional mode (Seuthe et al., 2011; Flynn et al., 2013) and motility to exploit vertical gradients in e.g. light and nutrients makes ciliates and dinoflagellates particularly well-adapted to the stratified summer months.

The trend towards net heterotrophy is further amplified by the seasonal increase in mesozooplankton biomass which exceeded protist biomass in summer by roughly one order of magnitude. The seasonal increase in mesozooplankton biomass was largely driven by the calanoid copepods *C. finmarchicus* and *C. glacialis* and can be explained by a combination of ontogenetic growth and advection from the adjacent shelf. Advection of AW during summer is a major conduit of zooplankton into Kongsfjorden (Basedow et al., 2004). The fact that the majority of zooplankton taxa that dominate in summer have a predominantly herbivorous feeding mode also suggests that a large fraction of summer primary production is ingested by copepods, either feeding directly on phytoplankton or indirectly by feeding on heterotrophic and mixotrophic protist grazers of small phytoplankton. Bivalvia veligers were the dominant meroplankton in summer which is in line with earlier findings from Svalbard (Kwasniewski et al., 2013; Stübner et al., 2016;

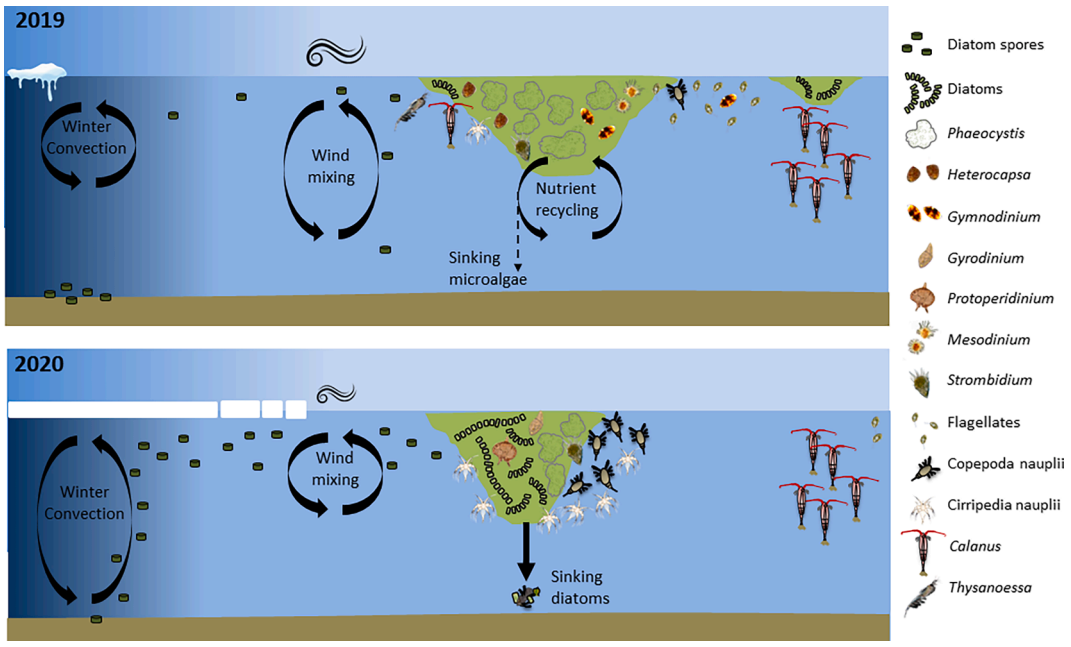

Fig. 14. Schematic representation of the two bloom scenarios in 2019 and 2020 with the main environmental drivers and plankton taxa represented.

Søreide et al., 2022). They preferentially feed on small algae < 10 μm congruent with the dominance of small-sized flagellates during summer. The shelled pteropod *Limacina helicina* was the dominant macrozooplankton in summer. This species is known to peak in summer when reproduction takes place (Gannefors et al., 2005) and can occur in dense swarms. This is consistent with our findings and indicates that we captured aggregations of this species which can be an important food source for higher trophic level organisms, including baleen whales (Comeau et al., 2010). The peak of *L. helicina* in late summer 2020 was accompanied by the highest standing stocks of the predatory pteropod *Clione limacina* which suggests a predator–prey relationship (Böer et al., 2005).

4.6. Conclusions

Our study suggests that selective grazing by *Calanus* copepods, advected into Kongsfjorden, on the inoculum of the dominant spring bloom diatoms, possibly in combination with less efficient resuspension of diatom resting spores, favored *Phaeocystis pouchetii* in spring 2019 (Fig. 14). There is evidence from both field data (Lasternas and Agusti, 2010; Nöthig et al., 2015; Assmy et al., 2017) and satellite observations (Orkney et al., 2020) for an increased dominance of *Phaeocystis* in the Atlantic sector of the Arctic Ocean. Our data indicate that a shift towards increased dominance of *Phaeocystis* will likely lead to a weakening of the biological carbon pump (Fig. 14). There seems to be a better zooplankton recruitment, particularly in the two dominant *Calanus* copepod species, associated with the diatom-dominated spring bloom (Fig. 14). Our study hence suggests that a floristic shift from diatoms towards *Phaeocystis* will result in more carbon being channeled to the microbial loop and dissolved organic matter pool than to the "classical" food web and the benthos. Importantly, spring bloom composition also impacted the summer plankton community as illustrated by the late summer diatom bloom in 2019 fueled by residual silicic acid not used up during the *Phaeocystis*-dominated spring bloom. Otherwise, the nutrient-poor summer months are characterized by small-sized phytoplankton and ciliates and dinoflagellates with mixo- or heterotrophic feeding modes and peak biomass of mesozooplankton grazers dominated by *Calanus finmarchicus* and *C. glacialis* exerting strong top-down control on the protist community.

Given the different fates of spring-bloom diatoms and *Phaeocystis* for the carbon cycle and marine food webs, the need to address the species level in biogeochemical and ecosystem studies should be obvious and can be illustrated by the following thought experiment: If all viable diatom cells at the start of the 2020 bloom had accumulated at rates equal to *Thalassiosira nordenskioeldii* (0.33 d^{-1}), the diatom standing stock we measured on 19 May would have been reached by 8 May and on 19 May it would have attained 163 g C m^{-2} (if nutrient supply had been unlimited) instead of the 8 g C m^{-2} we recorded. Conversely, the lower early bloom abundances and accumulation rates of the bloom-forming *Thalassiosira* species compared to *Phaeocystis pouchetii* in 2019 allowed the latter species to draw down 94% of the nitrate inventory within 20 days (based on the measured POC to PON molar ratio applied to *P. pouchetii* carbon biomass). This illustrates that the ecosystem role of the bloom-forming diatoms is unlikely to be filled by other diatom taxa as reflected in the recurrent annual patterns of spring bloom succession (von Quillfeldt 2000) and that any reduction in the inoculum of the spring bloom diatoms will have far-reaching consequences for carbon sequestration and trophic transfer.

Author contributions

PA wrote the paper with input from all co-authors. The study design involved PA, AB, HH, ACK, CJMH and AW. Field sampling from Ny-Ålesund was conducted by ACK, AB, KKEW and CJMH in 2019 and by ACK in 2020. Phyto- and zooplankton and biogeochemistry samples were taken by JW, AT, HH and AW during the RV *Lance* cruise in August 2019 and by PA, AB, HH, AW, OP and PD during the RV *Kronprins Haakon* cruise in July 2020. MC and AF contributed the DIC data. LMG analyzed chlorophyll *a* satellite imagery. Microscopic analysis of protist community samples was carried out by AT and JMW. Zooplankton analysis was conducted by WP and SK. Meteorological data were contributed by MM, sea ice data by OP and oceanographic mooring data by DDT. All authors contributed to data interpretation and to the writing of the manuscript.

Funding

Kongsfjorden seasonal pelagic monitoring was funded through the Norwegian Polar Institute's Svalbard program and the Fram Centre Ocean Acidification Flagship. Protist taxonomy analyses were partly

funded by the Polish Ministry of Science and Higher Education (projects W28/Svalbard/2019 and W37/Svalbard/2020).

Declaration of Competing Interest

The authors declare that they have no known competing financial interests or personal relationships that could have appeared to influence the work reported in this paper.

Data availability

Data will be made available on request.

Acknowledgements

We thank Amalia Keck Al-Habahbeh, Fieke Rader, Laura Wischnewski, Kristin Heggland, Claire Mourgues, Peter Leopold, Mikko Vihtakari, Piotr Kuklinski, personnel of Sverdrup and AWIPEV stations and Kings Bay AS for field and cruise support and Lucie Goraguer for producing Figs. 5 and 13 and Marika Marnela for help with Fig. 3.

Appendix A. Supplementary data

Supplementary data to this article can be found online at https://doi.org/10.1016/j.pocean.2023.102996.

References

Archer, S.D., Verity, P.G., Stefels, J., 2000. The impact of microzooplankton on the progression and fate of the spring bloom in fjords of northern Norway. Aquat. Microb. Ecol. 22, 27–42.

Ardyna, M., Arrigo, K.R., 2020. Phytoplankton dynamics in a changing Arctic Ocean. Nat. Clim. Change 10, 892–903. https://doi.org/10.1038/s41558-020-0905-y.

Ardyna, M., Babin, M., Gosselin, M., et al., 2014. Recent Arctic Ocean sea ice loss triggers novel fall phytoplankton blooms. Geophys. Res. Lett. 41, 6207–6212.

Ardyna, M., Mundy, C.J., Mills, M.M., et al., 2020. Environmental drivers of under-ice phytoplankton bloom dynamics in the Arctic Ocean. Elem. Sci. Anth. 8, 30. https://doi.org/10.1525/elementa.430.

Arrigo, K.R., DiTullio, G.R., Dunbar, R.B., et al., 2000. Phytoplankton taxonomic variability in nutrient utilization and primary production in the Ross Sea. J. Geophys. Res. Oceans 105, 8827–8846.

Arrigo, K.R., van Dijken, G.L., 2015. Continued increases in Arctic Ocean primary production. Prog. Oceanogr. 136, 60–70. https://doi.org/10.1016/j.pocean.2015.05.002.

Assmy, P., Smetacek, V., Montresor, M., et al., 2013. Thick-shelled, grazer-protected diatoms decouple ocean carbon and silicon cycles in the iron-limited Antarctic Circumpolar Current. Proc. Nat. Acad. Sci. USA 110, 20633–20638.

Assmy, P., Fernández-Méndez, M., Duarte, P., et al., 2017. Leads in Arctic pack ice enable early phytoplankton blooms below snow-covered sea ice. Sci. Rep. 7, 40850. https://doi.org/10.1038/srep40850.

Assmy, P., Smetacek, V., Montresor, M., Ferrante, M.I., 2019. Algal blooms. In: Schaechter, M. (Ed.), Encyclopedia of Microbiology, fourth ed. Academic Press, pp. 61–76.

Backhaus, J.O., Wehde, H., Hegseth, E.N., Kampf, J., 1999. 'Phyto-convection': the role of oceanic convection in primary production. Mar. Ecol. Prog. Ser. 189, 77–92.

Backhaus, J.O., Hegseth, E.N., Wehde, H., et al., 2003. Convection and primary production in winter. Mar. Ecol. Prog. Ser. 251, 1–14.

Bae, S., Kim, H., Nam, S.I., Choi, K.H., Kim, T.W., Yun, S.T., Kim, H.S., Kim, T.H., Han, D., Ko, Y.H., Kim, J.H., Lim, Y.K., Park, J.M., 2022. The composition and abundance of phytoplankton after the spring bloom in the Arctic Svalbard fjords. Estuar. Coast. Shelf Sci. 275, 107970. https://doi.org/10.1016/j.ecss.2022.107970.

Basedow, S.L., Eiane, K., Tverberg, V., Spindler, M., 2004. Advection of zooplankton in an Arctic fjord (Kongsfjorden, Svalbard). Estuar. Coast. Shelf Sci. 60, 113–124.

Behrenfeld, M.J., 2010. Abandoning Sverdrup's Critical Depth Hypothesis on phytoplankton blooms. Ecology 91, 977–989.

Beine, H.J., Argentini, S., Maurizi, A., et al., 2001. The local wind field at Ny-Ålesund and the Zeppelin mountain at Svalbard. Meteorog. Atmos. Phys. 78, 107–113. https://doi.org/10.1007/s007030170009.

Bérard-Therriault, L., Poulin, M., Bossé, L. 1999. Guide d'identification du phytoplancton marin de l'estuaire et du golfe du Saint-Laurent: incluant également certains protozoaires. Publ. Spec. Can. Sci. Halieut. Aquat. 128, 387 pp.

Berge, J., Heggland, K., Lønne, O.J., et al., 2015. First records of Atlantic mackerel (*Scomber scombrus*) from the Svalbard archipelago, Norway, with possible explanations for the extension of its distribution. Arctic 68, 54–61. http://dx.doi.org/10.14430/arctic4455.

Bhaskar, J.T., Parli, B.V., Tripathy, S.C., Jawak, S.D., Varunan, T., 2023. Does suspended sediment affect the phytoplankton community composition and diversity in an Arctic fjord? A comparative study during summer. Environ. Monit. Assess 195, 168. https://doi.org/10.1007/s10661-022-10734-0.

Bischof, K., Convey, P., Duarte, P., et al., 2019. Kongsfjorden as harbinger of the future Arctic: knowns, unknowns and research priorities. In: Hop, H., Wiencke, C. (Eds.), The ecosystem of Kongsfjorden, Svalbard. Advances in Polar Ecology 2. Springer, Cham, pp. 537–562. https://doi.org/10.1007/978-3-319-46425-1_14.

Böer, M., Gannefors, C., Kattner, G., et al., 2005. The Arctic pteropod *Clione limacina*: seasonal lipid dynamics and life strategy. Mar. Biol. 147, 707–717.

Brown, T.A., Hegseth, E.N., Belt, S.T., 2015. A biomarker-based investigation of the mid-winter ecosystem in Rijpfjorden. Svalbard. Polar Biol. 38, 37–50.

Calbet, A., Saiz, E., 2005. The ciliate-copepod link in marine ecosystems. Aquatic Microb. Ecol. 38, 157–167.

Carvalho, F., Kohut, J., Oliver, M.J., Schofield, O., 2017. Defining the ecologically relevant mixed-layer depth for Antarctica's coastal seas. Geophys. Res. Lett. 44, 338–345.

Castellani, C., Irigoien, X., Harris, R.P., Lampitt, R.S., 2005. Feeding and egg production of *Oithona similis* in the North Atlantic. Mar. Ecol. Prog. Ser. 288, 173–182.

Comeau, S., Jeffree, R., Teyssié, J.-L., Gattuso, J.-P., 2010. Response of the Arctic pteropod *Limacina helicina* to projected future environmental conditions. PLoS ONE 5 (6), e11362.

Cottier, F., Tverberg, V., Inall, M., et al., 2005. Water mass modification in an Arctic fjord through cross-shelf exchange: the seasonal hydrography of Kongsfjorden. Svalbard. J. Geophys. Res. 110, C12005. https://doi.org/10.11029/12004JC002757.

Dabrowska, A.M., Wiktor, J.M., Wiktor Jr, J.M., et al., 2021. When a year is not enough: Further study of the seasonality of planktonic protist communities structure in an ice-free high Arctic fjord (Adventfjorden, West Spitsbergen). Water 13, 1990. https://doi.org/10.3390/w13141990.

Dalpadado, P., Arrigo, K.R., van Dijken, G.L., et al., 2020. Climate effects on temporal and spatial dynamics of phytoplankton and zooplankton in the Barents Sea. Prog. Oceanogr. 185, 102320.

Degerlund, M., Eilertsen, H.C., 2010. Main species characteristics of phytoplankton spring blooms in NE Atlantic and Arctic waters (68–80°N). Estuar. Coasts 33, 242–269.

Descamps, S., Strøm, H., 2021. As the Arctic becomes boreal: ongoing shifts in a high-Arctic seabird community. Ecology 102, e03485.

Descamps, S., Aars, J., Fuglei, E., et al., 2017. Climate change impacts on wildlife in a High Arctic archipelago – Svalbard. Norway. Glob. Clim. Biol. 23, 490–502.

Dickson, A.G., Sabine, C.L., Christian, J.R., (Eds.), 2007. Guide to best practices for ocean CO_2 measurements. PICES Special Publication 3, pp. 191.

Duarte, P., Weslawski, J.M., Hop, H., 2019. Outline of an Arctic fjord ecosystem model for Kongsfjorden-Krossfjorden, Svalbard. In: Hop, H., Wiencke, C. (Eds.), The ecosystem of Kongsfjorden, Svalbard. Advances in Polar Ecology 2. Springer, Cham, pp. 485–514.

Dybwad, C., Assmy, P., Olsen, L.M., et al., 2021. Carbon export in the seasonal sea ice zone north of Svalbard from winter to late summer. Front Mar. Sci. 7, 252800. https://doi.org/10.3389/fmars.2020.525800.

Edler, L., Elbrächter, M., 2010. The Utermöhl method for quantitative phytoplankton analysis. Intergovernmental Oceanographic Commission of UNESCO.

Eilertsen, H.C., Taasen, J.P., Weslawski, J.M., 1989. Phytoplankton studies in the fjords of West Spitzbergen: Physical environment and production in spring and summer. J. Plankton Res. 11, 1245–1260.

Eilertsen, H.C., Wyatt, T., 2000. Phytoplankton models and life history strategies. South African J. Mar. Sci. 22, 323–338.

Flynn, K.J., Stoecker, D.K., Mitra, A., et al., 2013. Misuse of the phytoplankton-zooplankton dichotomy: the need to assign organisms as mixotrophs within plankton functional types. J. Plankton Res. 35, 3–11.

Fossheim, M., Primicerio, R., Johannesen, E., et al., 2015. Recent warming leads to a rapid borealization of fish communities in the Arctic. Nat. Clim. Change 5, 673–677. https://doi.org/10.1038/nclimate2647.

Fransson, A., Chierici, M., Hop, H., et al., 2016. Late winter- to-summer change in ocean acidification state in Kongsfjorden, with implications for calcifying organisms. Polar Biol. 39, 1841–1857. https://doi.org/10.1007/s00300-016-1955-5.

Gaebler-Schwarz, S., Davidson, A., Assmy, P., et al., 2010. A new cell stage in the haploid-diploid life cycle of the colony-forming haptophyte *Phaeocystis antarctica* and its ecological implications. J. Phycol. 46, 1006–1016.

Gannefors, C., Böer, M., Kattner, G., et al., 2005. The Arctic butterfly *Limacina helicina*: lipids and life strategy. Mar. Biol. 147, 169–177.

Gerland, S., Pavlova, O., Divine, D., et al. , 2020. Long-term monitoring of landfast sea ice extent and thickness in Kongsfjorden, and related applications (FastIce). In: Van den Heuvel et al. (Eds.): SESS report 2019, Svalbard Integrated Arctic Earth Observing System, Longyearbyen, Chapter 6. pp. 160-167.

Gerland, S., Renner, A.H.H., 2007. Sea ice mass balance in an Arctic fjord. Ann. Glaciol. 46, 435–442.

Gerland, S., Pavlova, O., Marnela, M., et al., 2022. Sea ice extent variability in Kongsfjorden, Svalbard during 2003–2021, based on visual observations from the mountain Zeppelinfjellet. Norwegian Polar Institute. https://data.npolar.no/dataset/d6d31f5b-8413-42b4-9736-db88d55816dc.

Gilstad, M., Sakshaug, E., 1990. Growth-rates of 10 diatom species from the Barents Sea at different irradiances and day lengths. Mar. Ecol. Prog. Ser. 64, 169–173.

Gluchowska, M., Kwasniewski, S., Prominska, A., et al., 2016. Zooplankton in Svalbard fjords on the Atlantic-Arctic boundary. Polar Biol. 39, 1785–1802.

Grote, U., Pasternak, A., Arashkevich, E., et al., 2015. Thermal response of ingestion and egestion rates in the Arctic copepod *Calanus glacialis* and possible metabolic consequences in a warming ocean. Polar Biol. 38, 1025–1033.

Halbach, L., Vihtakari, M., Duarte, P., et al., 2019. Tidewater glaciers and bedrock characteristics control the phytoplankton growth environment in an Arctic fjord. Front. Mar. Sci. 6, 254. https://doi.org/10.3389/fmars.2019.00254.
Hansen, P.J., 1992. Prey size selection, feeding rates and growth dynamics of heterotrophic dinoflagellates with special emphasis on *Gyrodinium spirale*. Mar. Biol. 114, 327–331.
Hanssen-Bauer, I., Førland, E.J., Hisdal, H., et al., (Eds.) 2019. Climate in Svalbard 2100 - a knowledge base for climate adaptation. Norway, Norwegian Centre of Climate Services (NCCS) for Norwegian Environment Agency (Miljødirektoratet), 208 pp. http://dx.doi.org/10.25607/OBP-888.
Hasle, G.R., Heimdal, B.R., 1998. The net phytoplankton in Kongsfjorden, Svalbard, July 1988, with general remarks on species composition of arctic phytoplankton. Polar Research 17, 31–52.
Haug, T., Falk-Petersen, S., Greenacre, M., et al., 2017. Trophic levels and fatty acids in harp seals compared with common minke whales in the Barents Sea. Mar. Biol. Res. 13, 919–923.
Hegseth, E.N., Assmy, P., Wiktor, J., et al., 2019. Phytoplankton seasonal dynamics in Kongsfjorden, Svalbard and the adjacent shelf. In: Hop, H., Wiencke, C. (Eds.), The ecosystem of Kongsfjorden, Svalbard. Advances in Polar Ecology 2, Springer, Cham. pp. 173–227. http://dx.doi.org/10.1007/978-3-319-46425-1_6.
Hegseth, E.N., Tverberg, V., 2013. Effect of Atlantic water inflow on timing of the phytoplankton spring bloom in a high Arctic fjord (Kongsfjorden, Svalbard). J. Mar. Syst. 113, 94–105.
Highfield, J.M., Eloire, D., Conway, D.V.P., et al., 2010. Seasonal dynamics of meroplankton assemblages at station L4. J Plankton Res 32, 681–691.
Hillebrand, H., Durselen, C.D., Kirschtel, D., et al., 1999. Biovolume calculation for pelagic and benthic microalgae. J. Phycol. 35, 403–424.
Hodal, H., Falk-Petersen, S., Hop, H., et al., 2012. Spring bloom dynamics in Kongsfjorden, Svalbard: Nutrients, phytoplankton, protozoans and primary production. Polar Biol. 35, 191–203.
Holm-Hansen, O., Riemann, B., 1978. Chlorophyll *a* determination: Improvement of the methodology. Oikos 30, 438–447.
Hop, H., Assmy, P., Wold, A., et al., 2019. Pelagic ecosystem characteristics across the Atlantic Water Boundary Current from Rijpfjorden, Svalbard, to the Arctic Ocean during summer (2010–2014). Front. Mar. Sci. 6, 181. https://doi.org/10.3389/fmars.2019.00181.
Hop, H., Wold, A., Vihtakari, M., et al., 2019a. Zooplankton in Kongsfjorden (1996-2016) in relation to climate change. In: Hop, H., Wiencke, C. (Eds.), The ecosystem of Kongsfjorden, Svalbard, Advances in Polar Ecology 2, Springer, Cham. pp. 229-303. http://dx.doi: 10.1007/978-3-319-46425-1_7.
Hop, H., Wiencke, C. (Eds.), 2019. The Ecosystem of Kongsfjorden, Svalbard. Springer, Cham. https://doi.org/10.1007/978-3-319-46425-1.
Hop, H., Pearson, T., Hegseth, E.N., et al., 2002. The marine ecosystem of Kongsfjorden. Svalbard. Polar Res. 21, 167–208.
Hovelsrud, G.K., Veland, S., Kaltenborn, B., et al., 2021. Sustainable Tourism in Svalbard: Balancing economic growth, sustainability, and environmental governance. Polar Rec. 57, 1–7. https://doi.org/10.1017/S0032247421000668.
Huntely, M., Tande, K., Eilertsen, H.C., 1987. On the trophic fate of *Phaeocystis pouchetii* (Hariot). II. Grazing rates of *Calanus hyperboreus* (Krøyer) on diatoms and different size categories of *Phaeocystis pouchetii*. J. Exp. Mar. Biol. Ecol. 110, 197–212. https://doi.org/10.1016/0022-0981(87)90001-3.
Ingvaldsen, R.B., Assmann, K.M., Primicerio, R., et al., 2021. Physical manifestations and ecological implications of Arctic Atlantification. Nat. Rev. Earth Environ. 2, 874–889.
Irigoien, X., Flynn, K.J., Harris, R.P., 2005. Phytoplankton blooms: a 'loophole' in microzooplankton grazing impact? J. Plankton Res. 27, 313–321.
Isaksen, K., Nordli, Ø., Ivanov, B., et al., 2022. Exceptional warming over the Barents area. Sci. Rep. 12, 9371. https://doi.org/10.1038/s41598-022-13568-5.
Jacobson, D.M., Anderson, D.M., 1986. Thecate heterotrophic dinoflagellates: Feeding behavior and mechanisms. J. Phycol. 22, 249–258.
Jakobsson, M., Mayer, L., Coakley, B., Dowdeswell, J.A., Forbes, S., Fridman, B., Hodnesdal, H., Noormets, R., Pedersen, R., Rebesco, M., Schenke, H.W., 2012. The international bathymetric chart of the Arctic Ocean (IBCAO) version 3.0. Geophys. Res. Lett. 39 (12), L12609.
Jeong, H.J., Latz, M.I., 1994. Growth and grazing rates of the heterotrophic dinoflagellates *Protoperidinium* spp. on red tide dinoflagellates. Mar. Ecol. Prog. Ser. 106, 173–185.
Johnson, M.L., Lakowicz, J.R., Joshi, N., Gryzcynski, I., 1987. Transient effects in quenching detected by harmonic-content frequency-domain fluorometry. Biophys. J. 51, A286.
Kohlbach, D., Hop, H., Wold, A., et al., 2021. Multiple trophic markers trace dietary carbon sources in Barents Sea zooplankton during late summer. Front. Mar. Sci. 7, 610248. https://doi.org/10.3389/fmars.2020.610248.
Konik, M., Darecki, M., Pavlov, A.K., et al., 2021. Darkening of the Svalbard fjords waters observed with satellite ocean color imagery in 1997–2019. Front. Mar. Sci. 8, 699318. https://doi.org/10.3389/fmars.2021.699318.
Kubiszyn, A.M., Wiktor, J.M., 2016. The *Gymnodinium* and *Gyrodinium* (Dinoflagellata: Gymnodiniaceae) of the West Spitsbergen waters (1999–2010): biodiversity and morphological description of unidentified species. Polar Biol. 39, 1739–1747.
Kubiszyn, A.M., Wiktor, J.M., Wiktor Jr, J.M., et al., 2017. The annual planktonic protist community structure in an ice-free high Arctic fjord (Adventfjorden, West Spitsbergen). J. Mar. Syst. 169, 61–72.
Kwasniewski, S., Hop, H., Falk-Petersen, S., Pedersen, G., 2003. Distribution of *Calanus* species in Kongsfjorden, a glacial fjord in Svalbard. J. Plankton Res. 25, 1–20.
Kwasniewski, S., Walkusz, W., Cottier, F., Leu, E., 2013. Mesozooplankton dynamics in relation to food availability during spring and early summer in a high latitude glaciated fjord (Kongsfjorden), with focus on *Calanus*. J. Mar. Syst. 111–112, 83–96.
Lalande, C., Moriceau, B., Leynaert, A., et al., 2016. Spatial and temporal variability in export fluxes of biogenic matter in Kongsfjorden. Polar Biol. 39, 1725–1738.
Lampe, V., Nöthig, E.-M., Schartau, M., 2021. Spatio-temporal variations in community size structure of Arctic protist plankton in the Fram Strait. Front. Mar. Sci. 7, 1239. https://doi.org/10.3389/fmars.2020.579880.
Landry, M.R., Calbet, A., 2004. Microzooplankton production in the oceans. ICES J. Mar. Sci. 61, 501–507.
Lasternas, S., Agusti, S., 2010. Phytoplankton community structure during the record Arctic ice-melting of summer 2007. Polar Biol. 33, 1709–1717.
Lavrentyev, P.J., Franzè, G., Moore, F.B., 2019. Microzooplankton distribution and dynamics in the Eastern Fram Strait and the Arctic Ocean in May and August 2014. Front. Mar. Sci. 6, 264. https://doi.org/10.3389/fmars.2019.00264.
Lefort, K.J., Garroway, C.J., Ferguson, S.H., et al., 2020. Killer whale abundance and predicted narwhal consumption in the Canadian Arctic. Glob. Change. Biol. 26, 4276–4283.
Li, W.K.W., McLaughlin, F.A., Lovejoy, C., Carmack, E.C., 2009. Smallest algae thrive as the Arctic Ocean freshens. Science 326, 539.
Löder, M.G.J., Meunier, C., Wiltshire, K.H., et al., 2011. The role of ciliates, heterotrophic dinoflagellates and copepods in structuring spring plankton communities at Helgoland Roads, North Sea. Mar. Biol. 158, 1551–1580.
Löder, M.G.J., Kraberg, A.C., Aberle, N., et al., 2012. Dinoflagellates and ciliates at Helgoland Roads, North Sea. Helgol. Mar. Res. 66, 11–23.
Long, J.D., Smalley, G.W., Barsby, T., et al., 2007. Chemical cues induce consumer-specific defenses in a bloom-forming marine phytoplankton. Proc. Natl. Acad. Sci. USA 104, 10512–10517.
Luhtala, H., Tolvanen, H., 2013. Optimizing the use of Secchi depth as a proxy for euphotic depth in coastal waters: An Empirical Study from the Baltic Sea. ISPRS Int. J. Geo-Inf. 2, 1153–1168.
Lydersen, C., Assmy, P., Falk-Petersen, S., et al., 2014. The importance of tidewater glaciers for marine mammals and seabirds in Svalbard. Norway. J. Mar. Syst. 129, 452–471.
Marquardt, M., Vader, A., Stüner, E.I., et al., 2016. Strong seasonality of marine microbial eukaryotes in a high-Arctic fjord (Isfjorden, in West-Spitsbergen, Norway). Appl. Environ. Microbiol. 82, 1868–1880.
Maturilli, M., Hanssen-Bauer, I., Neuber, R., et al., 2019. The atmosphere above Ny-Ålesund: Climate and global warming, ozone and surface UV radiation. In: Hop, H., Wiencke, C. (Eds.) The ecosystem of Kongsfjorden, Svalbard. Advances in Polar Ecology 2. Springer, Cham, pp. 23-47. http://dx.doi: 10.1007/978-3-319-46425-1_2.
Maturilli, M., Herber, A., König-Langlo, G., 2013. Climatology and time series of surface meteorology in Ny-Ålesund. Svalbard. Earth Syst. Sci. Data 5, 155–163. https://doi.org/10.5194/essd-5-155-2013.
Meire, L., Meire, P., Struyf, E., et al., 2016. High export of dissolved silica from the Greenland Ice Sheet. Geophys. Res. Lett. 43, 9173–9182. https://doi.org/10.1002/2016GL070191.
Menden-Deuer, S., Lessard, E.J., 2000. Carbon to volume relationships for dinoflagellates, diatoms, and other protist plankton. Limnol. Oceanogr. 45, 569–579.
Metfies, K., von Appen, W.J., Kilias, E., et al., 2016. Biogeography and photosynthetic biomass of Arctic marine pico-eukaroytes during summer of the record sea ice minimum 2012. Plos One 11 (2).
Mohamed, B., Nilsen, F., Skogseth, R., 2022. Marine heatwaves characteristics in the Barents Sea based on high resolution satellite data (1982–2020). Front. Mar. Sci. 9, 821646 https://doi.org/10.3389/fmars.2022.821646.
Njestgard, J.C., Tang, K.W., Steinke, M., et al., 2007. Zooplankton grazing on *Phaeocystis*: a quantitative review and future challenges. Biogeochemistry 83, 147–172.
Nöthig, E.-M., Bracher, A., Engel, A., et al., 2015. Summertime plankton ecology in Fram Strait-a compilation of long- and short-term observations. Polar Res. 34 (1), 23349. https://doi.org/10.3402/polar.v34.23349.
Okolodkov, Y.B., 1993. Dinoflagellates from the Norwegian, Greenland and Barents Seas, and the Faroe—Shetland Islands area collected in the cruise of R/V „Oceania", in June-July 1991. Polish Polar Res. 14, 9–24.
Orkney, A., Platt, T., Narayanaswamy, B.E., et al., 2020. Bio-optical evidence for increasing *Phaeocystis* dominance in the Barents Sea. Philos. Trans. Roy. Soc. Math. Phys. Eng. Sci. 378 https://doi.org/10.1098/rsta.2019.0357.
Orkney, A., Sathyendranath, S., Jackson, T., Porter, M., Bouman, H.A., 2022. Atlantic inflow is the primary driver of remotely sensed autumn blooms in the Barents Sea. Mar. Ecol. Prog. Ser. 701, 25–40. https://doi.org/10.3354/meps14201.
Ormanczyk, M.R., Gluchowska, M., Olszewska, A., Kwasniewski, S., 2017. Zooplankton structure in high latitude fjords with contrasting oceanography (Hornsund and Kongsfjorden, Spitsbergen). Oceanologia 59, 508–524.
Østby, T.I., Vikhamar Schuler, T., Hagen, J.O., et al., 2017. Diagnosing the decline in climatic mass balance of glaciers in Svalbard over 1957–2014. Cryosphere 11, 191–215.
Oziel, L., Baudena, A., Ardyna, M., et al., 2020. Faster Atlantic currents drive poleward expansion of temperate phytoplankton in the Arctic Ocean. Nat. Comm. 11, 1705.
Paulsen, M.L., Doré, H., Garczarek, L., et al., 2016. *Synechococcus* in the Atlantic Gateway to the Arctic Ocean. Front. Mar. Sci. 3, 191. https://doi.org/ 10.3389/fmars.2016.00191.
Pavlova, O., Gerland, S., Hop, H., 2019. Changes in sea-ice extent and thickness in Kongsfjorden, Svalbard (2003-2016). In Hop, H., Wiencke, C. (Eds.), The ecosystem of Kongsfjorden, Svalbard. Advances in Polar Ecology 2, Springer, Cham. pp. 105-136. 10.1007/978-3-319-46425-1_4. http://dx.doi: 10.1007/978-3-319-46425-1_4.
Peperzak, L., Colijn, F., Gieskes, W.W.C., Peeters, J.C.H., 1998. Development of the diatom-*Phaeocystis* spring bloom in the Dutch coastal zone of the North Sea: the

silicon depletion versus the daily irradiance threshold hypothesis. J. Plankton Res. 20, 517–537.
Piwosz, K., Walkusz, W., Hapter, R., et al., 2009. Comparison of productivity and phytoplankton in warm (Kongsfjorden) and a cold (Hornsund) Spitsbergen fjord in mid-summer 2002. Polar Biol. 32, 549–559.
Piwosz, K., Spich, K., Calkiewics, J., et al., 2015. Distribution of small phytoflagellates along an Arctic fjord transect. Environ. Microbiol. 17, 2393–2406.
Postel, L., Fock, H., Hagen, W., 2000. Biomass and abundance. In: Harris, R., Wiebe, P., Lens, J., Skjoldal, H.R., Huntley, M. (Eds.), ICES zooplankton methodology manual. Academic Press, San Diego, pp. 83–192.
Prominska, A., Cisek, M., Walczowski, W., 2017. Kongsfjorden and Hornsund hydrography — comparative study based on a multiyear survey in fjords of west Spitsbergen. Oceanologia 59, 397–412.
Reigstad, M., Wassmann, P., 2007. Does *Phaeocystis* spp. contribute significantly to vertical export of organic carbon? Biogeochemistry 83, 217–234.
Reigstad, M., Wassmann, P., Wexels Riser, C., et al., 2002. Variations in hydrography, nutrients and chlorophyll *a* in the marginal ice zone and the central Barents Sea. J. Mar. Syst. 38, 9–29.
Rey, F., Skjoldal, H.R., 1987. Consumption of silicic acid below the euphotic zone by sedimenting diatom blooms in the Barents Sea. Mar. Ecol. Prog. Ser. 36, 307–312.
Rokkan Iversen, K.R., Seuthe, L., 2011. Seasonal microbial processes in a high-latitude fjord (Kongsfjorden, Svalbard): I. Heterotrophic bacteria, picoplankton and nanoflagellates. Polar Biol. 34, 731–749.
Rynearson, T.A., Richardson, K., Lampitt, R.S., et al., 2013. Major contribution of diatom resting spores to vertical flux in the sub-polar North Atlantic. Deep Sea Res. I 82, 60–71.
Saenko, O.A., Flato, M., Weaver, A.J., et al., 2002. Improved representation of sea-ice processes in climate models. Atmos. Ocean. 40, 21–43.
Saito, H., Ota, T., Suzuki, K., Nishioka, J., Tsuda, A., 2006. Role of heterotrophic dinoflagellate *Gyrodinium* sp. in the fate of an iron induced diatom bloom. Geophys. Res. Lett. 33 (9), L09602. https://doi.org/10.1029/2005GL025366.
Saiz, E., Calbet, A., 2011. Copepod feeding in the ocean: scaling patterns, composition of their diet and the bias of estimates due to microzooplankton grazing during incubations. Hydrobiologia 666, 181–196.
Seuthe, L., Rokkan Iversen, K., Narcy, F., 2011. Microbial processes in a high-latitude fjord (Kongsfjorden, Svalbard): II. Ciliates and dinoflagellates. Polar Biol. 34, 751–766.
Siddons, B.L., Glegg, G., McQuatters-Gollop, A., 2018. Inter-regional coherence: Can Northeast Atlantic pelagic habitat indicators be applied to the Arctic? Mar. Policy 96, 53–64.
Skjoldal, H.R., Wiebe, P.H., Postel, L., et al., 2013. Intercomparison of zooplankton (net) sampling systems: results from the ICES/GLOBEC sea-going workshop. Prog. Oceanogr. 108, 1–42. https://doi.org/10.1016/j.pocean.2012.10.006.
Smetacek, V., 1985. Role of sinking in diatom life-history cycles: ecological, evolutionary and geological significance. Mar. Biol. 84, 239–251.
Smetacek, V., Henjes, J., Assmy, P., 2004. The role of grazing in structuring Southern Ocean pelagic ecosystems and biogeochemical cycles. Antarctic Sci. 16, 541–558.
Smetacek, V., Klaas, C., Strass, V.H., et al., 2012. Deep carbon export from a Southern Ocean iron-fertilized diatom bloom. Nature 487, 313–319.
Søreide, J.E., Leu, E., Berge, J., et al., 2010. Timing in blooms, algal food quality and *Calanus glacialis* reproduction and growth in a changing Arctic. Glob. Change Biol. 16, 3154–3163.
Søreide, J.E., Pitusi, V., Vader, A., et al., 2020. Environmental status of Svalbard coastal waters: coastscapes and focal ecosystem components (SvalCoast). SESS Report - State of Environmental Science in Svalbard. https://doi.org/10.5281/zenodo.4293849.
Søreide, J.E., Dmoch, K., Blachowiak-Samolyk, K., Trudnowska, E., Daase, M., 2022. Seasonal mesozooplankton patterns and timing of life history events in high-arctic fjord environments. Front. Mar. Sci. 9, 933461. https://doi.org/10.3389/fmars.2022.933461.
Starr, M., Himmelman, J.H., Therriault, J.C., 1991. Coupling of nauplii release in barnacles with phytoplankton blooms - a parallel strategy to that of spawning in urchins and mussels. J Plankton Res. 13, 561–571.
Stelfox-Widdicombe, C.E., Archer, S.D., Burkill, P.H., Stefels, J., 2004. Microzooplankton grazing in *Phaeocystis* and diatom-dominated waters in the southern North Sea in spring. J. Sea Res. 51 (1), 37–51.
Stoecker, D.K., Lavrentyev, P.J., 2018. Mixotrophic plankton in the polar seas: A pan-Arctic review. Front. Mar. Sci. 5, 292. https://doi.org/10.3389/fmars.2018.00292.
Stübner, E.I., Søreide, J.E., Reigstad, M., et al., 2016. Year-round meroplankton dynamics in high-Arctic Svalbard. J. Plankton Res. 38, 522–536.
Svendsen, H., Beszczynska-Møller, A., Hagen, J.O., et al., 2002. The physical environment of Kongsfjorden-Krossfjorden an Arctic fjord system in Svalbard. Polar Res. 21, 133–166.
Svensen, C., Vernet, M., 2016. Production of dissolved organic carbon by *Oithona nana* (Copepoda: Cyclopoida) grazing on two species of dinoflagellates. Mar. Biol. 163, 237..
Svensen, C., Halvorsen, E., Vernet, M., et al., 2019. Zooplankton communities associated with new and regenerated primary production in the Atlantic inflow North of Svalbard. Front. Mar. Sci. 6, 293. https://doi.org/10.3389/fmars.2019.0029.
Tang, K.W., Jakobsen, H.H., Visser, A.W., 2001. *Phaeocystis globosa* (Prymnesiophyceae) and the planktonic food web: Feeding, growth, and trophic interactions among grazers. Limnol. Oceanogr. 46, 1860–1870.
Throndsen, J., Hasle, G.R., Tangen, K., 2007. Phytoplankton of Norwegian Coastal Waters. Almater Forlag AS, 343 pp.
Tomas, C.R. (Ed.). (1997). Identifying Marine Phytoplankton. Elsevier, 858 pp. https://doi.org/10.1016/B978-0-12-693018-4.X5000-9.
Tverberg, V., Skogseth, R., Cottier, F., et al., 2019. The Kongsfjorden Transect: seasonal and inter-annual variability in hydrography. In: Hop, H., Wiencke, C. (Eds.), The ecosystem of Kongsfjorden, Svalbard. Advances in Polar Ecology 2. Springer, Cham, pp. 49–104. https://doi.org/10.1007/978-3-319-46425-1_3.
Utermöhl, H., 1958. Zur Vervollkommung der quantitativen Phytoplankton-Methodik. Mitt. Int. Ver. Theor. Angew. Limnol. 9, 1–38.
Vader, A., Marquardt, M., Meshram, A.R., Gabrielsen, T.M., 2015. Key Arctic phototrophs are widespread in the polar night. Polar Biol. 38, 13–21.
van de Poll, W.H., Abdullah, E., Visser, R.J.W., et al., 2020. Taxon-specific dark survival of diatoms and flagellates affects Arctic phytoplankton composition during the polar night and early spring. Limnol. Oceanogr. 65, 903–914. https://doi.org/10.1002/lno.11355.
van de Poll, W.H., Maat, D.S., Fischer, P., et al., 2021. Solar radiation and solar radiation driven cycles in warming and freshwater discharge control seasonal and inter-annual phytoplankton chlorophyll *a* and taxonomic composition in a high Arctic fjord (Kongsfjorden, Spitsbergen). Limnol. Oceanogr. 66, 1221–1236.
Verity, P.G., Brussaard, C.P., Nejstgaard, J.C., et al., 2007. Current understanding of *Phaeocystis* ecology and biogeochemistry, and perspectives for future research. Biogeochemistry 83, 1–3.
Vihtakari, M., 2020. PlotSvalbard: PlotSvalbard - Plot research data from Svalbard omaps. R package version (9), 2. https://github.com/MikkoVihtakari/PlotSvalbard.
von Quillfeldt, C.H., 2000. Common diatom species in arctic spring blooms: Their distribution and abundance. Bot. Mar. 43, 499–516.
von Quillfeldt, C.H., 2001. Identification of some easily confused common diatom species in arctic spring blooms. Bot. Mar. 44, 375–389.
Vonnahme, T.R., Persson, E., Dietrich, U., et al., 2021. Early spring subglacial discharge plumes fuel under-ice primary production at a Svalbard tidewater glacier. Cryosphere 15, 2083–2107.
Walkusz, W., Kwaśniewski, S., Falk-Petersen, S., et al., 2009. Seasonal and spatial changes in the zooplankton community in Kongsfjorden. Svalbard. Polar Res. 28, 254–281.
Weisse, T., Scheffel-Möser, U., 1990. Growth and grazing loss rates in single-celled *Phaeocystis* sp. (Prymnesiophyceae). Mar. Biol. 106, 153–158.
Wiedmann, I., 2010. Germination potential and spatial distribution of diatom resting stages in northern Norwegian fjords. University of Tromsø. MSc thesis, 68 pp.
Wiedmann, I., Ceballos-Romero, E., Villa-Alfageme, M., et al., 2020. Arctic observations identify phytoplankton community composition as driver of carbon flux attenuation. Geophys. Res. Lett. 47, e2020GL087465. https://doi. org/10.1029/2020GL08746.
Wiktor, J., Okolodkov, Y., Vinogradova, K., 1995. Atlas of the Marine Flora of Southern Spitsbergen. Ecology Group, Institute of Oceanology, Polish Academy of Sciences.
Wollenburg, J.E., Katlein, C., Nehrke, G., et al., 2018. Ballasting by cryogenic gypsum enhances carbon export in a *Phaeocystis* under-ice bloom. Sci. Rep. 8, 7703. https://doi.org/10.1038/s41598-018-26016-0.
Xing, X.G., Claustre, H., Blain, S., et al., 2012. Quenching correction for in vivo chlorophyll fluorescence acquired by autonomous platforms: A case study with instrumented elephant seals in the Kerguelen region (Southern Ocean). Limnol. Oceanogr. Meth. 10, 483–495.